Observability-Driven Hybrid Free-Field Reconstruction from In-Room Rotating-DUT Measurements

PHYSICAL LAB · Senden, Germany
Research manuscript

Abstract

Reconstructing a loudspeaker's free-field radiation from measurements in an ordinary room is an inverse problem involving source dynamics, reflected fields, geometry and measurement references. The PHYSICAL LAB research programme examines a practical acquisition consisting of six room-fixed receiver configurations and 72 known orientations of a rotating device under test. This paper consolidates its analytic, numerical and real-development evidence into a target-observability framework. A stationary degree-three outgoing/regular spherical model provides a controlled counterexample: its 432-by-32 pressure operator has rank 30 and two target-changing null directions. Correct multi-pose modelling distinguishes information supplied by rotation, eccentric source motion and physically imposed source–room coupling. Eccentricity can lift finite-model rank without making the inverse stable. Additional source-sensitive observations are consequently evaluated through their coupling to the missing target directions, with uncertainty and model discrepancy retained. Synthetic studies show that the required local sensor count depends strongly on the admissible source class, that co-rotation does not remove constant reflection contamination, and that secondary radiators can invalidate a cone-only low-frequency estimate. Geometric room scans constrain surfaces and candidate paths but do not measure acoustic boundary properties; precision local registration and broad room coverage serve different purposes. Time gating is analysed through both discarded direct-source response and retained reflections, leading to a target-qualified, covariance- and bias-aware hybrid architecture rather than a universal crossover frequency. Existing real data support accurate angular total-pressure prediction, not certified source/room separation. The proposed next stage is experimental qualification of a small registered source-assisted system, supported by independent numerical and physical references. The contribution is a defensible measurement architecture and its validity criteria, not a completed free-field product.

Keywords: inverse acoustics; sound-field separation; target observability; rotating loudspeaker; spherical harmonics; source-state sensing; room geometry; metrology; time gating; uncertainty.

Research status. Real physical DUT/room component certification remains **ABSTAIN**. Proposed hardware and frequency boundaries are not frozen. New MATLAB and COMSOL comparisons remain unexecuted in the current evidence set. The earlier V3.63p MATLAB result belongs to its historical implementation only [1–6].

Contents

1. Introduction

A loudspeaker measured in a room does not reveal its isolated radiation through a simple superposition of an identifiable “good” response and an identifiable “bad” response. The recorded pressure includes direct radiation, boundary reflections, room resonances, scattering and the effects of the complete measurement chain. These contributions can share spatial and temporal signatures. An inverse model can fit their sum very accurately while assigning the wrong contributions to the loudspeaker and the room. The central question is therefore not whether a corrected frequency response can be drawn, but whether the observations contain enough information to determine the requested physical quantity [2–4].

The desired result is often represented by a complex directional pressure, $p_{\mathrm{free}}(R\hat{\mathbf{u}}, f)$, or a far-field amplitude $F(\hat{\mathbf{u}}, f)$ at a declared coordinate and reference. Such data would support directivity development, comparison of prototypes, virtual receiver evaluation and correlation with electroacoustic simulation. The word *free-field* requires care. An outgoing field attributed to a source domain in the measured room is not necessarily the response that the same device would produce in an anechoic environment at unchanged electrical drive. Incident sound can scatter from the enclosure and can change the radiating motion. Recovering that counterfactual requires additional assumptions or source-state information, not merely a successful pressure decomposition [2–4,14].

The PHYSICAL LAB programme investigates whether controlled DUT rotation, a small set of receiver configurations, limited source-state assistance, geometric room information and qualified time windows can be combined into a practical reconstruction method. The approach is deliberately target-specific. A method useful for normalized magnitude directivity may still be inadequate for absolute pressure, phase-sensitive continuation or physical direct/reflected separation. Those outcomes should not be hidden behind a single “reconstruction accuracy” number [3,4].

The research has progressed from identifying a concrete stationary inverse-problem ambiguity to modelling the actual pose-dependent acquisition, testing additional observables, and comparing source, room and metrology assumptions. The resulting evidence suggests a frequency-dependent hybrid system. Low-frequency source and room information can constrain an inverse model where gating is inadequate. At frequencies where a time window has a qualified direct-field error, that estimate can be used instead. Where both methods estimate the same target in a common reference, their uncertainties and biases can determine a controlled transition. This is an emerging architecture, not an experimental claim that the full reconstruction is already achieved [3,4].

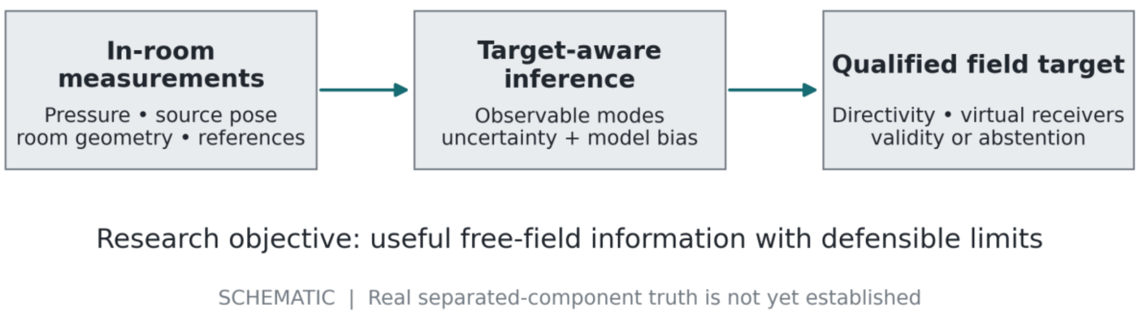

Figure 1. Research objective and evidence boundary. In-room observations are used to infer a declared field target through observable state directions and a quantified uncertainty budget. The final block is a proposed qualified output, not an experimentally established real-DUT free-field result. Evidence: schematic synthesis of the programme in [1–4].

This paper develops the mathematical chain behind that architecture. It begins with the physical acquisition and a finite-dimensional target criterion, then distinguishes rotational coding, eccentricity and source–room constraints. It examines where local sensing, electrical information and metrology add useful information, and where they do not. The final sections formulate a hybrid estimator, interpret the existing real-data boundary and define a focused physical-validation programme. Numerical results are selected for their explanatory value rather than as a catalogue of every exploratory configuration.

2. Position within inverse-acoustic measurement methods

Near-field acoustic holography provides an established framework for reconstructing radiation from spatial observations, rather than limiting analysis to pressures at the microphone positions. Its foundational formulation and subsequent developments motivate the use of wave-consistent representations and explicit continuation targets [7]. That motivation does not imply that an arbitrary sparse acquisition satisfies a uniqueness theorem. The source class, measurement aperture, available observables and noise model remain essential.

Several complementary method families are relevant. Sparse equivalent-source methods use a restricted or compressible source representation; the published C-ESM work explicitly discusses column coherence and the conditioning of near-field reconstruction [11]. Statistically optimized near-field acoustical holography addresses finite-aperture prediction through a wave-based transfer formulation and includes estimates of its validity region [23]. Pressure–velocity and double-layer methods introduce additional field observables and source-domain structure [9,10]. Boundary-element free-field recovery can support more flexible measurement positions, but still requires its particular physical and representation assumptions [22]. These are alternative sources of structure, not interchangeable guarantees for the present data.

Published commercial documentation also already distinguishes low-frequency field separation from higher-frequency time-window processing [18]. The general idea of using different methods in different frequency regions is therefore not claimed as a first invention here. The specific research question is how to qualify such an architecture for the actual rotating-DUT acquisition, uncertain manual geometry, source-state assistance and target-dependent missing directions. No proprietary algorithm, benchmark superiority or replacement for an established commercial scanner is claimed.

Current primary research continues to develop geometry- and physics-informed reconstruction. Boundary-informed Bayesian work incorporates uncertain boundary geometry and impedance-related priors [15]. Differentiable ESM jointly adjusts equivalent-source positions and strengths while enforcing geometric feasibility [16]. These are relevant potential tools for restricting a model or estimating its parameters. Their existence does not establish that the PHYSICAL LAB acquisition becomes identifiable for an unrestricted source and room. The target-kernel and robustness tests remain necessary regardless of the optimizer or representation.

The literature review is targeted rather than a systematic meta-analysis. Full-text, official-documentation and abstract-only access are distinguished in the reference inventory. External sources establish methodological context; the acquisition-specific ranks, sensor comparisons and error figures in this paper come from the supplied PHYSICAL LAB records [1–6].

3. Acquisition, evidence and coordinate conventions

3.1 Six physical configurations, not 432 room microphones

The frozen acquisition contract describes six physical receiver configurations, with the microphone fixed in the room during each angular scan and the DUT rotated through 72 unique orientations. The microphone was repositioned between scans, primarily in radius and height. The description does not assert six simultaneous microphone channels. Each original scan contains 73 records including the repeated angular seam, yielding 438 original records and 432 unique receiver–pose combinations [1,3].

The nominal room-frame coordinates, relative to the stated turntable/tweeter datum, are given in Table 1. These are manual engineering coordinates, not traceable metrology. The 72 unique angles run from $-180°$ to $175°$ in $5°$ increments. An unchanged gain setting and approximately unchanged room configuration are useful acquisition facts, but do not establish a traceable common complex gain or time origin between all scans [1,3].

Table 1. Nominal receiver configurations in frozen contract sequence. All coordinates are in metres.

Receiver s	x_s	y_s	z_s
1	1.000	0.000	0.000
2	1.500	0.000	0.000
3	1.500	0.000	−0.250
4	1.000	0.000	−0.250
5	1.000	0.000	−0.500
6	1.500	0.000	−0.500

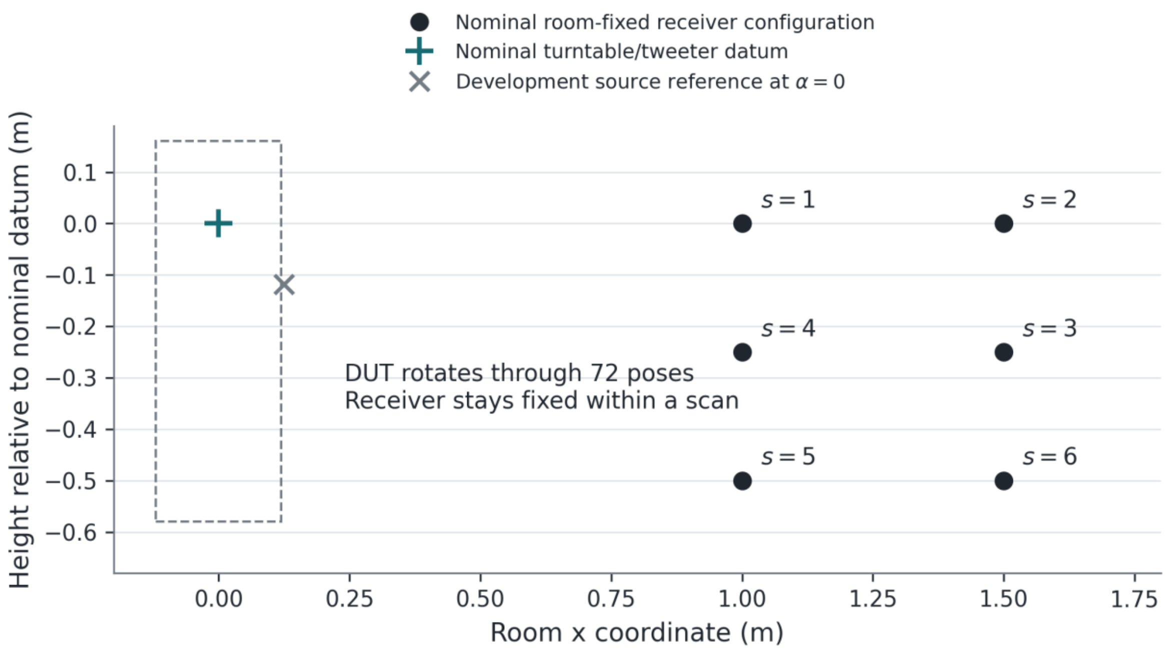

Figure 2. Side projection of the six nominal room-fixed receiver configurations. The source-reference marker at zero DUT angle uses the later timing-derived development estimate; the dashed DUT outline is schematic. A receiver is fixed during its scan, while the DUT rotates. Neither the drawing nor the tabulated coordinates establishes exact metrology or simultaneous six-channel acquisition [1,3,5].

A physically correct data object is $y_{s,n}(f)$, indexed by receiver configuration s, DUT pose n and frequency f. Let $\mathbf{t}$ denote a fixed room-frame turntable origin, $R_n \in SO(3)$ the known body-to-room rotation and $\mathbf{d}$ a body-frame source-reference offset. The corresponding source-frame evaluation vector and room-frame source centre are

$$\mathbf{r}_{s,n} = R_n^{\top}(\mathbf{x}_s - \mathbf{t}) - \mathbf{d}, \qquad \mathbf{c}_n = \mathbf{t} + R_n \mathbf{d}. \tag{1}$$

The changing $\mathbf{r}_{s,n}$ is a coordinate representation. It does not create a new physical room microphone. In particular, room boundaries do not co-rotate simply because the data are expressed in the DUT frame. Treating the 432 transformed coordinates as samples of one stationary external room field would change the physical experiment [1–4].

3.2 Acoustic reference and input-data identity

The later two-radius/three-plane geometry study supplies the development hypothesis $\mathbf{d} \approx (0.1249, -0.0012, -0.1178)$ m. It supersedes the earlier single-polar forward-offset estimate as the primary engineering reference. The fitted radial increment is approximately 496 mm. These values are inferred acoustically over the low/mid-frequency development band, not independently surveyed mechanical coordinates or a demonstrated frequency-independent acoustic centre [5].

The native acquisition uses a 96 kHz sampling rate and 131072-sample records. The stored CLIO spectrum and the transform of the full impulse response are distinct data products. The historical binary audit established that the stored spectrum includes windowing; the current studies preserve the full-IR lane separately. The vendor documentation likewise distinguishes time data from windowed or postprocessed frequency data [2–4,20]. A publication figure therefore has to identify its response lane, not merely call every complex array "the measurement".

The CLIO value 0.302 V denotes the output setting before the external power amplifier. It is not DUT terminal voltage. The approximate terminal-voltage recollection in the contract is not a calibrated electrical reference. Absolute acoustic sensitivity, channel response, source support and the actual radiator inventory remain unresolved where the supplied evidence does not establish them [1,3,4].

3.3 Evidence classification

Six labels are used throughout: **analytic result**, **verified numerical result**, **synthetic-model result**, **real development data**, **engineering inference** and **future research hypothesis**. A numerical synthetic result can have a verified implementation while still depending on an ideal source class. A real-data prediction result can be repeatable without identifying physical components. The distinction is essential to interpreting every table and figure.

The latest extended checkpoint and report define the current state [4]. Earlier controls and failed acceptance gates are preserved within their original scope. The historical 52/52 MATLAB handoff verifies its V3.63p research implementation, not the later Phase-II or extended code. The later 25-check and 20-check MATLAB harnesses remain unexecuted in the supplied state, as does COMSOL [3,4,6].

4. Physical field model and target definitions

The phasor convention is $\mathrm{Re}\{p(\mathbf{x}, f)e^{+i\omega t}\}$, where $\omega = 2\pi f$ and $k = \omega/c$. In a homogeneous source-free region, pressure obeys the Helmholtz equation and the outgoing Green function is

$$(\nabla^2 + k^2)p = 0, \qquad G(\mathbf{x}, \mathbf{s}; f) = \frac{e^{-ik\|\mathbf{x}-\mathbf{s}\|}}{4\pi\|\mathbf{x}-\mathbf{s}\|}. \tag{2}$$

The reference calculations use $c = 343$ m/s and $\rho_0 = 1.2$ kg/m^3. These are declared computational values, not measured environmental conditions. Spherical coordinates use polar angle ϑ from $+z$ and azimuth $\varphi = \mathrm{atan2}(y, x)$. Orthonormal complex spherical harmonics include the Condon–Shortley phase; coefficient ordering is first by degree l, then by $m = -l, \dots, l$ [2–4,8].

An outgoing/regular expansion in a declared source-free annulus can be written

$$p(\mathbf{r}, f) = \sum_{l=0}^{L} \sum_{m=-l}^{l} \left[a_{lm}(f)h_l^{(2)}(kr) + b_{lm}(f)j_l(kr)\right] Y_{lm}(\hat{\mathbf{r}}). \tag{3}$$

The outgoing term belongs to interior source support; the regular term represents an exterior-source field within its validity region. A regular spherical wave is not a purely converging singular Hankel wave. The annulus and enclosing source support are physical assumptions. In particular, a global outgoing series must not be evaluated inside a source-enclosing sphere and interpreted as a validated near-field radiator model. The local-source studies consequently use explicit local kernels or a surface integral instead [2,3].

The far-field target is defined by

$$p_{\mathrm{d}}(R\hat{\mathbf{u}}, f) \sim \frac{e^{-ikR}}{R} F(\hat{\mathbf{u}}, f), \qquad F(\hat{\mathbf{u}}, f) = \frac{1}{k} \sum_{l,m} i^{l+1} a_{lm}(f) Y_{lm}(\hat{\mathbf{u}}). \tag{4}$$

This separates far-field amplitude from pressure at a specified distance. A finite-distance target requires its own propagation operator and source-domain validity. Normalized directivity is a ratio relative to a declared nonzero direction, not a substitute for an absolute acoustic reference.

Table 2. Target hierarchy and the information each claim requires.

Target	Mathematical object	Additional interpretation requirement
Source coefficients	Selected entries of $\mathbf{q}$	Adequate and physically interpretable representation
Total pressure prediction	$B_{\mathrm{total}}\mathbf{q}$	Same total-field process and acquisition state
Direct pressure at measured poses	$B_{\mathrm{d}}\mathbf{q}$	Identifiable source/room attribution
Virtual receiver or far field	$B_{\mathrm{v}}\mathbf{q}$, $F(\hat{\mathbf{u}})$	Stable continuation in a valid domain
Normalized complex directivity	$F(\hat{\mathbf{u}})/F(\hat{\mathbf{u}}_0)$	Nonzero reference; common directional phase datum
Normalized magnitude directivity	$\lvert F(\hat{\mathbf{u}})/F(\hat{\mathbf{u}}_0)\rvert$	Phase is deliberately excluded from the target
Absolute free-field response	Calibrated direct/free-field target	Acoustic/electrical reference and justified source-state meaning
Anechoic response at unchanged drive	Counterfactual physical response	Loading, scattering and source-state transfer must be addressed

An algorithm can support one row of Table 2 and fail another. In particular, fitting total pressure at observed configurations does not by itself validate a field with the room removed. The source-domain versus counterfactual distinction is also recognized in published free-field recovery work that explicitly treats scattering [14].

5. Stationary six-ring control: a concrete ambiguity

The stationary reference is retained because it exposes a structural information deficit without relying on an optimizer’s behaviour. It is not the forward model of the rotating-DUT room experiment. In that control, two coaxial cylindrical radii and three heights form six complete pressure rings. At fixed cylindrical radius and height, spherical radius and polar angle are constant, so each spherical harmonic varies only as $e^{im\varphi}$ around the ring [2,3].

For a given azimuthal order m, the outgoing/regular degree-L model has $2(L - |m| + 1)$ complex coefficients. Each complete ring contributes only one complex Fourier coefficient for that m. Therefore the six-ring block has at most six independent equations, regardless of how densely the ring is sampled. Summing the deficits over angular orders gives

$$\operatorname{dimker}(A) \geq \sum_{m=-L}^{L} \max\{0, 2(L - |m| + 1) - 6\} = 2(L-2)^2, \qquad L \geq 3. \tag{5}$$

At $L = 3$, the deficit is in the axisymmetric $m = 0$ block: eight coefficients face six spatial equations. The reproduced full operator has 432 rows, 32 columns, rank 30 and nullity two. Its saved null directions have a normalized acquisition residual of approximately 4.17×10^{-16} and change the outgoing target. This establishes target ambiguity in the declared finite class, not merely a redundant coordinate description [3,4].

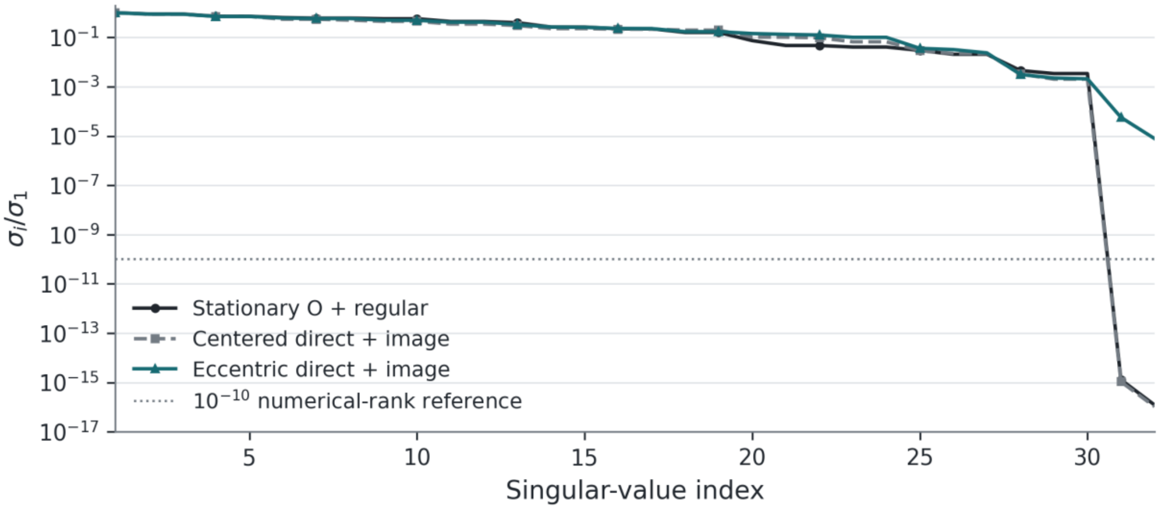

Figure 3. Supplied degree-three singular spectra at 1 kHz. The stationary outgoing/regular control and the centered independent direct/image relaxation retain two null directions. Eccentricity lifts the matched direct/image relaxation to rank 32, but its smallest singular values still imply severe instability. The 10^{-10} line is a numerical-rank diagnostic, not a universal physical noise threshold. Backing data: Phase-II 02_matched_singular_spectra.csv [3].

The counterexample does not say that all six-ring reconstruction is impossible. A sufficiently restricted known source class can be observable, and some lower-dimensional targets can be unique even when the coefficients are not. It does say that more angles on those same stationary traces cannot resolve the missing spatial equations for the stated general class. A smaller regularization penalty, a denser dictionary or a visually improved polar plot cannot overturn that rank argument.

The numerical witness normalization differs from the earlier Phase-I on-ring cancellation ratio of about 2.77×10^{-15}. A nullspace basis can be rotated and rescaled without changing the subspace. The reproducible scientific content is small $A\mathbf{v}$, nonzero target response $B\mathbf{v}$, and the axisymmetric modal interpretation—not equality of two differently normalized residual scalars [2,3].

6. Target observability, nullspace coupling and regularization

6.1 Exact finite-dimensional criterion

At one frequency, consider a declared admissible linear model

$$\mathbf{y} = A\mathbf{q} + \mathbf{e}, \qquad \mathbf{z} = B\mathbf{q}. \tag{6}$$

Proposition 1 — target observability. In the noiseless model, the target is uniquely determined by the measurements for every admissible state if and only if

$$\ker(A) \subseteq \ker(B). \tag{7}$$

Proof. Two states $\mathbf{q}_1$ and $\mathbf{q}_2$ produce the same data exactly when their difference $\mathbf{v} = \mathbf{q}_1 - \mathbf{q}_2$ satisfies $A\mathbf{v} = 0$. Their targets agree exactly when $B\mathbf{v} = 0$. Requiring target agreement for every data-equivalent pair is precisely the stated kernel inclusion. Conversely, a vector in $\ker(A)$ that is not in $\ker(B)$ supplies two indistinguishable states with different targets. This proves both directions [2–4].

Full coefficient rank is sufficient, but not necessary. For example, two equivalent-source coefficient sets may describe the same physical field in a declared region. Their representation difference is harmless for that field target. Conversely, a small residual for one estimated state does not test the full equivalence class of states that share the observations. Target observability concerns that equivalence class, not the appearance of a particular solution.

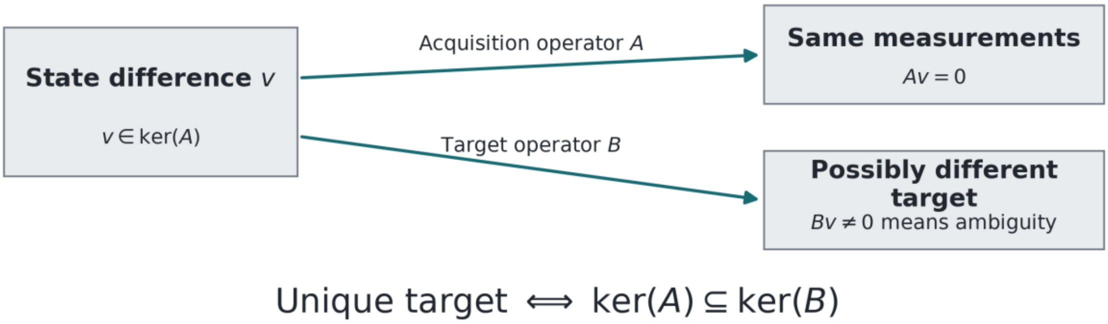

Figure 4. Physical meaning of target observability. An invisible state difference can leave the measurements unchanged while changing the desired output. The target is unique only if every acquisition-null direction is also target-null. This schematic does not depict a numerical spectrum or an experimental field [2–4].

6.2 What an additional sensor must observe

Let the columns of N span $\ker(A)$ in a declared coefficient metric. Adding observations $C\mathbf{q}$ leaves the original ambiguity $N\boldsymbol{\xi}$ admissible only when $CN\boldsymbol{\xi} = 0$. The exact augmented target condition is therefore

$$\ker(CN) \subseteq \ker(BN). \tag{8}$$

This follows directly by restricting Proposition 1 to the original nullspace. If every original null direction changes a relevant target, full column rank of CN removes that finite ambiguity. If some directions are target-irrelevant, observing all coefficient directions is unnecessary. A necessary dimension bound is $\mathrm{rank}(CN) \geq \mathrm{rank}(BN)$; equality of ranks alone is not sufficient, because the null directions must be the correct ones.

This formulation avoids equating missing dimension with physical microphone count. One sensor measured across controlled states can provide several independent rows; several sensors on a symmetry-degenerate layout can provide almost the same row. The relevant comparison includes the covariance of the added observations, their sensitivity to geometry, and their target response. A large unwhitened coupling value is not automatically useful when it comes from a noisy modality or a different unit scale [3,4].

6.3 Stabilization is not new information

A regularized inverse can select a stable member of an equivalence class. For example, a Tikhonov penalty favours small coefficients in its chosen metric. A sparse penalty favours a restricted representation. Both can be scientifically useful when the prior is justified, but neither converts an unobserved direction into measured information. The data-only kernel and the role of the prior must remain visible [2–4,11,21].

A particularly revealing negative control assigns an independent unknown contamination value to every new local pressure. The augmented operator is $\begin{bmatrix} A & 0 \\ C & I \end{bmatrix}$. For any $\mathbf{v} \in \ker(A)$, the state change $[\mathbf{v}; -C\mathbf{v}]$ remains invisible. Extra rows have been accompanied by enough new nuisance freedom to preserve the original ambiguity. Nearness to a radiator does not, by definition, remove that freedom; it must be reduced by physics or bounded discrepancy [3].

7. Rotation, eccentricity and shared-source constraints

For a centered rotation about the room z axis, spherical-harmonic evaluation gives

$$Y_{lm}(R_z(-\alpha)\hat{\mathbf{r}}) = e^{-im\alpha}Y_{lm}(\hat{\mathbf{r}}). \tag{9}$$

Thus known rotation separates angular characters m. It also ties all poses to a single intrinsic source state rather than introducing one arbitrary source vector per angle. However, the factor is exactly one for $m = 0$. Pure orientation diversity does not create new modulation within the axisymmetric sector. For an outgoing-only degree-six model, seven axisymmetric coefficients still face only six receiver configurations; the tested centered operator has rank 48 of 49 at 1 kHz [3,8].

General rotations can be represented by Wigner-D blocks acting within each harmonic degree. In the supplied research, rotation conventions are checked against direct coordinate evaluation. When the source reference is eccentric, the safest forward construction evaluates the basis at the correctly transformed source-centered coordinate. It need not approximate a translated expansion at the wrong origin. Any truncated addition-theorem representation would require its own convergence and domain check [3].

For a horizontal receiver $(R, 0, z_s)$ and body offset $\left(d_x, d_y, d_z\right)$, the path length obeys

$$\ell_{s,n}^2 = R^2 + d_x^2 + d_y^2 + (z_s - d_z)^2 - 2R\left(d_x\cos\alpha_n - d_y\sin\alpha_n\right). \tag{10}$$

This changes both propagation phase and observation direction. Figure 5 evaluates this expression using the later development offset; it is an explanatory calculation, not a new timing fit or a newly acquired measurement.

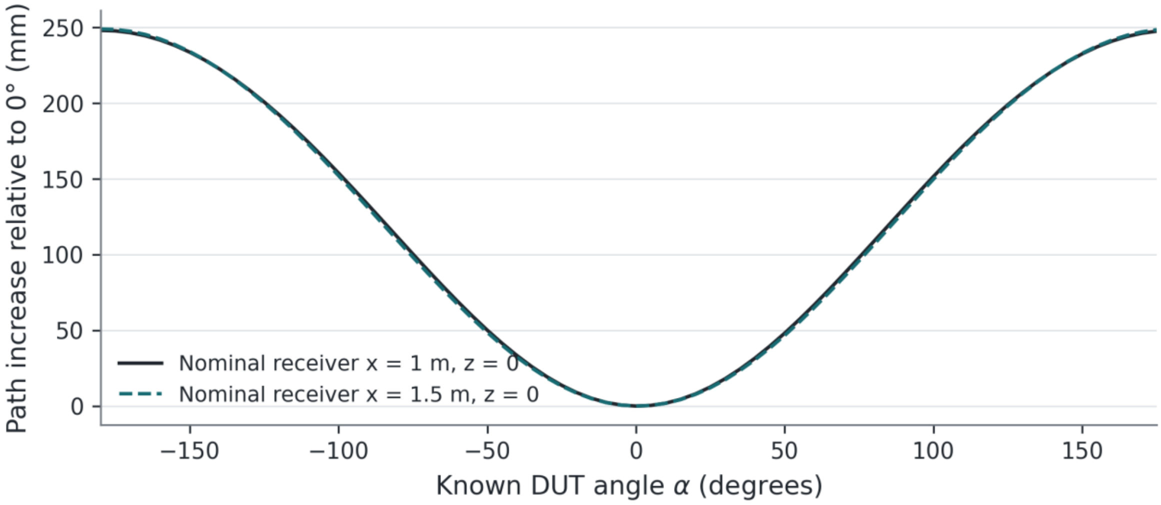

Figure 5. Path-length modulation caused by the development eccentricity at two nominal zero-height receivers. The curves use the explicit rigid-coordinate distance formula and the hypothesis $\mathbf{d} = (124.9, -1.2, -117.8)$ mm. They illustrate geometric modulation, not measured path truth or a frequency-independent source centre. Exact generated coordinates and distances are included in the publication data workbook [1,5].

Three mechanisms must be distinguished. Orientation changes modal angular signatures. Eccentricity changes propagation paths and directions. A source-linked room model reduces independent parameters by requiring reflected fields to arise from that same source. Comparing an independent 32-coefficient split with a known-coupling 16-coefficient model cannot attribute every improvement to rotation.

A matched 32-column direct/image relaxation isolates eccentricity without changing the parameter count. At 1 kHz, rank increases from 30 to 32, but the scaled condition number remains approximately 1.27 ×

10^5. By comparison, the degree-three outgoing-only source operator has condition numbers about 170.36 when centered and 96.36 with the development eccentricity. These are different model classes; the favourable direct-only result does not qualify an unknown-room split [3].

Angular sampling likewise depends on the model. On a uniform N-pose grid, orders congruent modulo N alias. For centered degree L, $N > 2L$ separates the angular characters, but the receiver geometry must still separate degrees within each m block. Rank saturation in a small model does not eliminate the benefit of additional independent noise averaging. Nor does it establish the pose count of a real high-frequency source whose spatial order is not yet validated.

8. Source–room and reference ambiguities

A fixed room is not a pose-invariant acoustic contribution. The rotating directional source illuminates boundaries differently, and eccentricity changes source-to-boundary paths. A physically structured model therefore links reflection operators to the same intrinsic source state. At a fixed frequency a useful finite form is

$$\mathbf{y} = \left[A_{\mathrm{d}}(\mathbf{g}) + \sum_{j=1}^{J} \beta_j \, E_j(\mathbf{g}) \right] \mathbf{a} + G_{\mathrm{res}} \mathbf{b}_{\mathrm{res}} + \mathbf{e}. \tag{11}$$

Here $\mathbf{g}$ contains geometry, E_j maps the rotating source through candidate path j, and β_j describes the path's acoustic response. The residual basis is explicitly constrained. For known geometry and fixed β_j, the problem is linear in $\mathbf{a}$. Unknown reflection coefficients make it bilinear or nonlinear; local Jacobian rank does not prove global uniqueness [3,4,21].

Two simplified room models explain the danger of excess freedom. A static complex residual at each physical receiver overlaps the centered source's unmodulated sector. A receiver-specific Fourier residual can overlap each source signature whose angular order it contains. At sufficient Fourier order it can absorb the centered finite source's complete rotational signature. Such models are useful negative controls, but a reduced total residual must not be interpreted as better component attribution [3].

Reference gauges are separate. If a common complex scale is unknown, multiplying the source by $\gamma \neq 0$ and dividing the reference gain by γ leaves the measured data unchanged. Absolute pressure and source coefficients change. A well-defined normalized complex ratio can cancel that scale, but cannot generally cancel all source-shape or geometric ambiguities.

For $z(\hat{\mathbf{u}}) = B\mathbf{q}/(\mathbf{b}_0\mathbf{q})$, the local derivative is

$$J_z = \frac{B - \mathbf{z}\mathbf{b}_0}{\mathbf{b}_0\mathbf{q}}, \qquad J_z\mathbf{q} = 0. \tag{12}$$

For a magnitude-only target away from zeros,

$$J_{|z|} = \frac{\mathrm{Re}\{\bar{z} J_z\}}{|z|}. \tag{13}$$

A translation can change the far-field phase by a direction-dependent factor while leaving its magnitude unchanged. Consequently normalized complex directivity and normalized magnitude directivity have different local observability requirements. In the matched 41-real-parameter acoustic-only model, the reported normalized-magnitude target has no changing exact-null direction, whereas the normalized-complex target retains one. That is a local, model-conditional result, not a certificate for an arbitrary real loudspeaker [4].

The 41-parameter comparison holds the source, reflection and nuisance state fixed across modalities. Its acoustic-only likelihood has rank 38. Registered local or room geometry raises the data rank to 39; an ideal independently calibrated pressure–velocity addition reaches rank 40. Calibrated local source observations can reach full local rank under their stated mappings. Removing those calibration assumptions or enlarging the source class changes the problem. A finite posterior after adding priors must not be substituted for these data-only statements [4].

9. Practical observability and uncertainty-aware linear algebra

Exact rank answers whether a finite target is unique in ideal arithmetic. Practical observability asks whether noise, nuisance variation and model discrepancy corrupt that target excessively. The analysis therefore whitens observations using a declared covariance, scales coefficient columns, and reports the singular spectrum before choosing regularization [2–4].

Let $W\Sigma W^{\mathrm{H}} = I$ on the supported observation space, and let D contain the nonzero column norms of WA, with explicit handling of zero columns. Write

$$A_s = WAD^{-1} = U\Lambda V^{\mathrm{H}}, \qquad N = D^{-1}V_0. \tag{14}$$

Here V_0 spans the scaled numerical-null directions and Λ contains singular values. The reference relative threshold is 10^{-10}; additional near-rank levels and the declared noise budgets assess weak directions. The threshold is a diagnostic convention, not a universal physical definition of zero. Very small symmetry-cancellation residue must not be normalized by its own tiny norm and promoted into a new observed mode.

On the retained subspace, the target-noise mapping is

$$M_B = BD^{-1}V_r\Lambda_r^{-1}U_r^{\mathrm{H}}W. \tag{15}$$

Its norm and singular values measure target amplification. If $BN \neq 0$, this finite mapping is not the complete target uncertainty: an unconstrained null amplitude can make the target arbitrarily different without changing the data. A physically justified bound or prior can restrict that ambiguity, but its contribution must be stated separately.

Linear nuisance columns are projected out after whitening. If U_η spans the whitened nuisance space, the source information is assessed with $\left(I - U_\eta U_\eta^{\mathrm{H}}\right)WA_{\mathrm{a}}$. Geometric parameters are real even when pressures are complex. Their Jacobians are therefore represented in a real-stacked likelihood. Circular complex noise with RMS standard deviation σ has real and imaginary variances $\sigma^2/2$; real geometry errors need not produce circular complex pressure errors [3,4].

Noise-only uncertainty, deterministic perturbation quantiles and worst-direction errors answer different questions. A small median over a prescribed set of sinusoidal perturbations can under-excite a damaging singular direction. The extended sensor study consequently retains analytic white-noise target RMS and worst-energy-direction diagnostics alongside scenario medians. None of these synthetic summaries is a population confidence interval for unmeasured laboratory errors [4].

10. A frequency-dependent division of reconstruction effort

The central architectural inference is to avoid requiring one method to solve the same inverse problem over the entire audio band. At low frequencies, source response and room response can overlap over long times, while a short reflection-free window may remove relevant dynamics. At other frequencies, a qualified window can provide the desired direct-field estimate with less dependence on a detailed room inverse. The transition depends on the target, source memory, path structure and uncertainties, not merely the number of acoustic cycles in a window [3,4].

A proposed system therefore has three operational regions. In a source-assisted region, a validated low-dimensional source state and a constrained room model support inversion. In a qualified overlap region, both inverse and gated estimates are available for the same physical target and reference. In a gating-dominated region, the windowed estimate satisfies an independently justified direct-field error budget. Unsupported frequencies remain unqualified rather than being filled by an attractive crossfade.

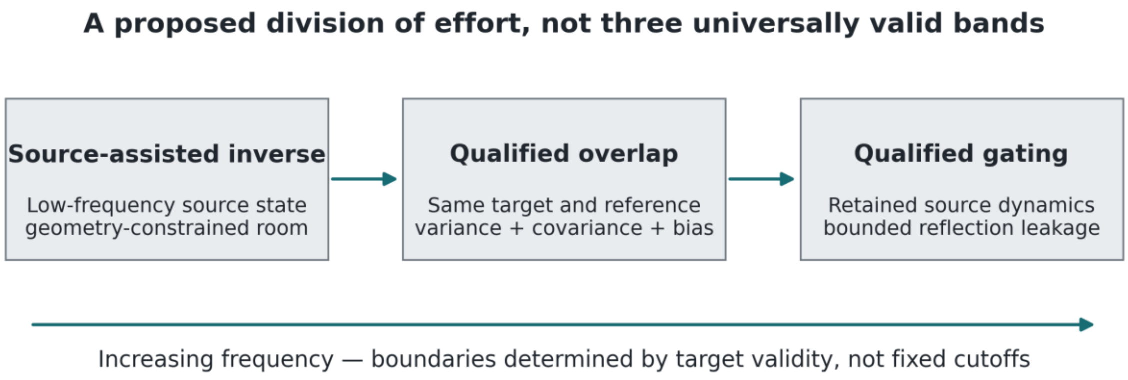

Figure 6. Proposed frequency-dependent reconstruction architecture. The low-frequency inverse, overlap and gated regions are defined by target validity and uncertainty. Their boundaries are deliberately not assigned universal frequencies. The scheme is an engineering inference from the numerical evidence, not a completed physical product algorithm [3,4].

The room representation can also change with the relevant physics and computation. A geometry-informed wave or modal model may be appropriate where room resonances dominate. A limited source-linked path model can describe identifiable early reflections. Gating may reduce the need for a detailed room model at higher frequencies. These are possible allocations of effort, not a claim that image solutions are intrinsically invalid at low frequency: an appropriate infinite rigid-plane image construction can be wave-exact [4,12].

The engineering attraction is selective complexity. Local source sensors need not surround every driver if higher-frequency targets are already qualified by another method. Conversely, a tweeter or midrange with long ringing or strong crossover interaction cannot be excluded simply because it is nominally a high-frequency radiator. The required source state must follow the error budget of the chosen band. The present real-data evidence does not yet define those takeover frequencies [4].

11. Gating: discarded source response and retained room response

Let the measured impulse response be $h = h_{\mathrm{d}} + h_{\mathrm{r}}$, where the subscripts denote the desired direct/source response and the unwanted room contribution under a declared physical decomposition. Applying a window $w(t)$ gives $H_{\mathrm{gate}} = \mathcal{F}\{wh\}$. The exact error identity is

$$H_{\mathrm{gate}} - H_{\mathrm{d}} = \mathcal{F}\{(w-1)h_{\mathrm{d}}\} + \mathcal{F}\{wh_{\mathrm{r}}\}. \tag{16}$$

The first term is source information discarded by the window. The second is room information retained within it. A window that ends before a candidate echo can still truncate a long source decay. A longer window can retain more source response while admitting an earlier reflection. These mechanisms affect magnitude, phase and directional ratios differently. A gate is therefore qualified for a target and tolerance, not simply for a nominal reflection-free duration [4].

The supplied synthetic campaign evaluates short-pulse, low-frequency-decay and long high-frequency-ringing source responses. For a 3 ms direct-to-reflection gap and a 2.55 ms tapered gate, the all-higher-tested-frequency pass boundaries are approximately 49.80 Hz, 312.01 Hz and 2634.52 Hz, respectively. The joint criteria are a 10% complex error, 1 dB magnitude error and 10° phase error on the sampled grid.

A three-cycle guide would give the same 1176.47 Hz value for all three cases, missing their different source dynamics [4].

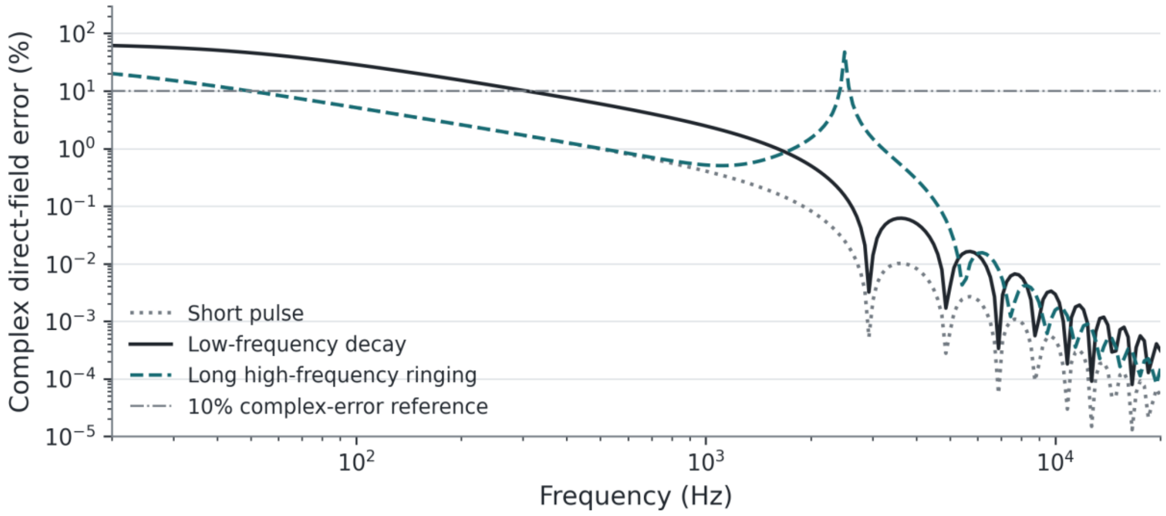

Figure 7. Gating error depends on source memory. All curves use the same synthetic 3 ms reflection gap and 2.55 ms tapered gate. The plotted quantity is complex direct-field error; the quoted pass boundaries also require the magnitude and phase criteria. The short-pulse, LF-decay and long-HF-ringing examples are not product crossover frequencies. Backing data: extended 13_gating_source_dependence.csv [4].

The low short-pulse boundary should not be interpreted as general low-frequency resolution from a 2.55 ms measurement. It is a result for a known rapidly decaying source response that is largely retained. The finite-record transform can sample many frequencies, but the ability to distinguish an unknown long-lived response is a separate question. Likewise, a high-frequency resonance can need a longer observation than a simple wavelength or retained-cycle argument suggests.

Real impulse responses do not arrive with independently labelled direct and reflected components. In the current corpus, changing the interval excluded around the direct cluster changes the next detected feature. That feature may contain source ringing, another radiator, diffraction or a reflection. The actual first-reflection identity and real gating transition remain unqualified. Agreement between several windows is useful stability evidence but is not proof that any of them retains all direct sound [4].

A practical gate-selection module should therefore retain candidate path identities, geometry uncertainty, source-tail hypotheses and the target error metric. It should test plausible alternatives rather than accepting the first peak returned by a detector. Optical geometry can narrow candidate delays, but cannot by itself determine the direct-source tail. The expected result is a band of supported gating decisions with explicit abstention where the evidence is insufficient.

12. Local low-frequency source-state assistance

Local measurements can supply independent constraints on source variables that the room acquisition observes weakly. The appropriate model is not “near-field pressure equals source truth”, but an additional observation with its own contamination and discrepancy:

$$\mathbf{z}_{\mathrm{NF}} = C_{\mathrm{a}}\mathbf{a} + C_{\mathrm{b}}\mathbf{b} + \boldsymbol{\delta}_{\mathrm{NF}} + \mathbf{e}_{\mathrm{NF}}. \quad (17)$$

When room and neighbouring-source terms are not represented explicitly, their omission belongs in $\boldsymbol{\delta}_{\mathrm{NF}}$, with a justified bound or model. A large local amplitude can improve signal-to-noise ratio, yet a steep local gradient can also increase placement sensitivity. The same measurement can be informative and difficult to register accurately [3,4].

The practical concept is a small number of fixed, registered or co-rotating observations near the lowest relevant radiator or radiators. It is not a demand for a dense manual near-field scan. A two-way system might require assistance mainly for its midwoofer; a three-way system might require it mainly for its woofer. These are hypotheses contingent on the qualified band, actual crossover and all materially radiating structures. Ports, passive radiators and cabinet radiation cannot be omitted because they lack an independent electrical drive [3,4].

For a linear finite model, permanent uncertainty-weighted observations preserve more information than using them only to initialize an otherwise ambiguous inverse. Removing the local term after initialization restores the original kernel. A joint whitened least-squares solution is preferable to unnecessary alternation when the model is linear. A nonlinear source–room iteration must have a defined objective and convergence test, but convergence itself is not a physical certificate.

The key design question is the smallest adequate source class. Table 3 compares source families at 63 Hz with a fixed physical noise reference within each family. The local counts are total added channels in that experiment, not a prescription of channels per real radiator. The scalar pair has two source coefficients plus six prescribed-bearing external-wave coefficients. The woofer/port class has four local woofer modes, one port coefficient and six external coefficients. The broader model has four modes at each of four source groups, plus six external coefficients [4].

Table 3. Source complexity and local sensing at 63 Hz. Analytic white-noise target RMS, not measured real-DUT errors.

Declared source/external class	Added local channels	Relative target RMS
Two scalar radiators, eight coefficients total	0	0.430%
Four woofer modes plus port, eleven coefficients total	2	1.269%
Four source groups, 22 coefficients total	2	56.440%
Same 22-coefficient class	4	19.700%
Same 22-coefficient class	6	11.582%

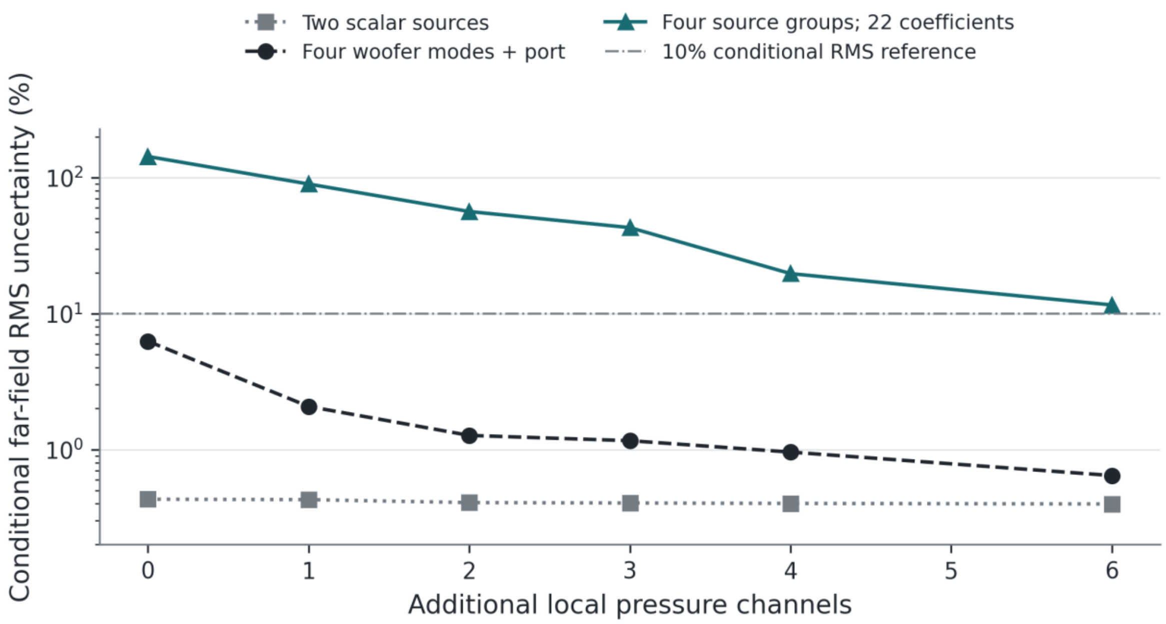

Figure 8. Sensor-count value depends on the admissible source class. The noise reference is fixed across counts within each class. The broader 22-coefficient model remains above the 10% conditional RMS reference with six local channels at 63 Hz. Different source classes are not different measurements of the same real loudspeaker. Backing data: extended 01_local_count_63Hz.csv [4].

A favourable scalar-source control and a weak multimode control are not contradictory. They identify a boundary in the assumptions. The correct sequence is to validate a minimal source representation on withheld spatial and pose observations, then choose the additional measurements that couple to its relevant missing modes. Selecting a sensor count first and subsequently choosing the easiest source model would reverse that logic.

13. Spatial modes, sensor placement and standoff

More local observations are useful only when they reveal different source combinations with sufficient signal-to-uncertainty ratio. Center-axis sampling gives a clear analytic example. Consider a circular disk of radius a in an infinite rigid baffle, with prescribed normal velocity

$$v(y,z) = q_0 + q_1 \frac{y}{a} + q_2 \frac{z}{a} + q_3 \left[2 \frac{y^2 + z^2}{a^2} - 1 \right]. \tag{18}$$

These four shapes represent a piston-like component, two odd rocking components and a radial-node component. For the selected phasor convention, pressure in the radiating half-space is given by the Rayleigh integral

$$p(\mathbf{x}) = \frac{i\rho_0\omega}{2\pi} \int_S v\,(\mathbf{s}) \frac{e^{-ik\|\mathbf{x}-\mathbf{s}\|}}{\|\mathbf{x}-\mathbf{s}\|}\, \mathrm{d}S. \tag{19}$$

At a point on the central axis, the kernel and the circular domain are even in both transverse coordinates. The integrals of y/a and z/a vanish. Any number of center-axis distances therefore remains blind to those odd modes. This is a symmetry argument, not an artifact of the numerical solver. The supplied implementation checks the piston term against an analytic on-axis expression and verifies quadrature refinement [3].

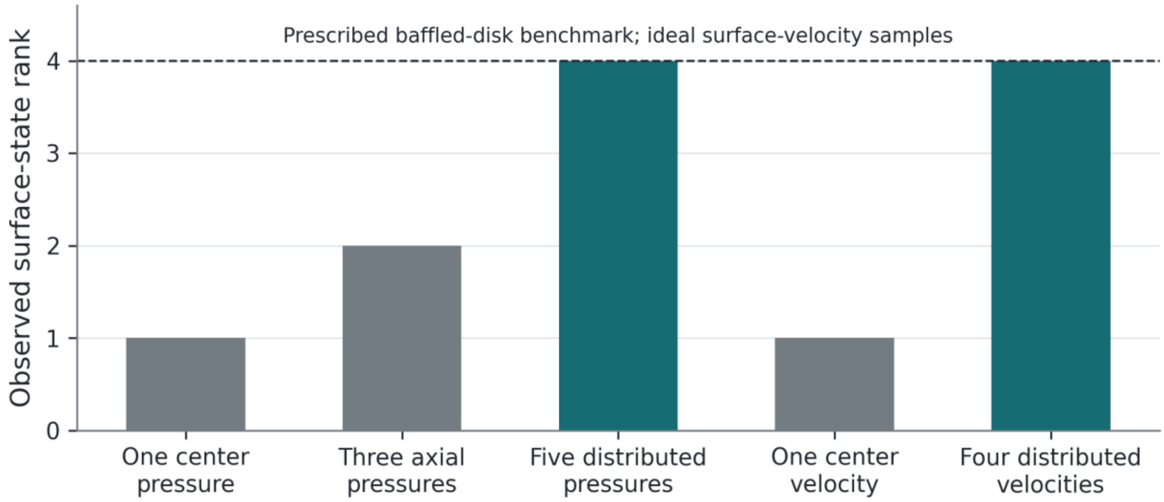

Figure 9. Spatial observability of four prescribed baffled-disk velocity modes. Three center-axis pressure distances observe only two modes; distributed pressure or surface-velocity samples observe all four in this finite model. A central surface-velocity measurement is not a complete source-state observation either. "Velocity" here denotes ideal source-surface samples, not calibrated real LDV measurements. Backing data: Phase-II 08_disk_observable_modes.csv [3].

The selected 80 mm radius disk at 1 kHz and 20 mm nominal standoff has rank one with a single center pressure, rank two with three axial distances, and rank four with five distributed pressures. Four suitable surface-velocity samples also have rank four. These are known-mode experiments, not a model of every real cone, suspension, dustcap or waveguide. Their significance is that geometric placement can be more important than repeating a measurement at several distances along a symmetry line [3].

A piston-only fit to one local pressure can have zero local residual while producing a biased far-field pattern when the true source contains higher modes. Accordingly, source-class validation should include observations withheld from the local fit and a target that is sensitive to the omitted motion. Individual-driver excitation can help identify source signatures, but cannot reveal a mode whose field vanishes at the selected point. Transferring a signature from individual excitation to complete loudspeaker operation also requires a stability and interaction check.

Standoff remains a design variable. Closer placement can increase source dominance and sensitivity to spatial detail, while increasing coordinate sensitivity, local contamination by nearby structures and loading risk. Farther placement changes mode weighting and can mix adjacent radiators. The supplied point-multipole and finite-disk studies do not select the same optimum. Neither 20 mm nor 40 mm is established as a universal value [3,4].

Finite aperture and probe disturbance must also be separated. A small package relative to wavelength may still disturb a strongly varying near field when it is close to a source. The extended rigid-sphere proxy quantifies this possibility, but is not the actual microphone's scattering correction. Mechanical minimization of disturbance and an independent full-wave or physical check remain necessary before a local channel is treated as non-perturbing [4,17].

14. Co-rotating sensing and correlated uncertainty

Fixing a local sensor relative to the DUT can reduce manual repositioning and maintain a known source–sensor geometry over the scan. This makes co-rotation a strong provisional implementation concept. It does not imply that the recorded pressure is independent of the room. A useful decomposition is

$$z_i(\alpha, f) = s_i(f) + r_i(\alpha, f) + e_i(\alpha, f), \qquad \overline{z}_i = s_i + \overline{r}_i + \overline{e}_i. \tag{20}$$

Only the varying part of the room contribution can be separated by angular variation alone. The mean reflected contribution remains. In the supplied floor-reflection example, an invariant contribution is indistinguishable from part of the stable source signature at one local observation. The tested one-channel, three-amplitude model observes only two amplitudes even with 72 poses [4].

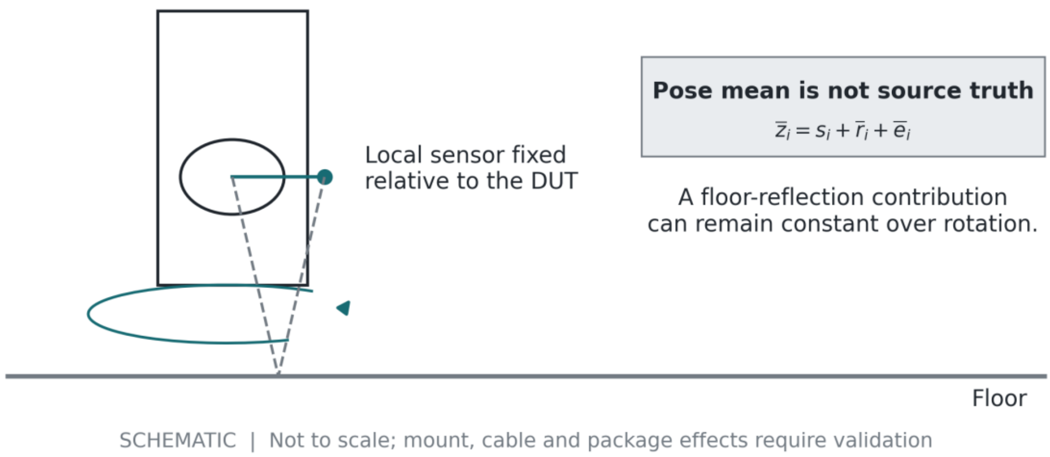

Figure 10. Proposed co-rotating local source monitor. Stable source–sensor geometry reduces repositioning, but a pose-invariant floor contribution can remain in the local mean. The diagram is a schematic, not a final mechanical design; source outline, stand, distances and path strength are not measured. Cable behaviour, mount repeatability and scattering remain validation tasks [4].

Repeated poses can reduce independent noise after rank has saturated. They do not average down a perfectly correlated reference error. For a simple scalar average with independent variance σ_{ind}^2 and a common variance σ_{com}^2,

$$\operatorname{var}(\overline{z}) = \frac{\sigma_{\text{ind}}^2}{N} + \sigma_{\text{com}}^2. \tag{21}$$

This illustrates why common timing, gain, calibration and geometric registration cannot be treated as independent noise on every sample. In the supplied 1% independent/2% common example, increasing pose count approaches a 2% uncertainty floor. The numerical percentages are assumptions in a covariance illustration, not measured MEMS channel specifications [4].

The proposed measurement should keep the local observations in the joint inverse with their common-reference covariance. It should also test whether source state drifts with time, whether cable motion creates a pose-dependent transfer, and whether the fixture itself changes the field. A later local measurement cannot automatically certify the historical source state or the earlier manually placed microphone coordinates. Combining old and new campaigns requires a documented transfer and repeatability experiment [3,4].

15. Secondary radiators and electrical source information

A low-frequency source representation should follow the radiating structures, not the number of electrical amplifier channels. For a vented enclosure, a useful restricted state is $\mathbf{a}_{\mathrm{LF}} = [a_{\mathrm{w}}, a_{\mathrm{p}}]^{\mathrm{T}}$ for woofer and port. For a passive-radiator system, the second state describes passive motion. Multiple woofers can be expressed through common and differential modes when the drive and geometry justify that representation [3,4].

The supplied coupled examples use a declared lumped electroacoustic model. With box compliance C_b, secondary-path impedance Z_{sec}, mechanical driver impedance Z_{ms} and cone area S_d, one convenient formulation is

$$Z_b = (i\omega C_b + Z_{\mathrm{sec}}^{-1})^{-1}, \qquad v_{\mathrm{w}} = \frac{B\ell\, I}{Z_{\mathrm{ms}} + S_d^2 Z_b}, \qquad V = Z_e I + B\ell\, v_{\mathrm{w}}. \tag{22}$$

The active and secondary volume velocities are then related through the same box state, with outward-radiation signs defined consistently. In a validated model, electrical observations can constrain that coupling. In an unvalidated one, the same relation is a source prior with uncertain parameters, not an exact observation of all acoustic motion.

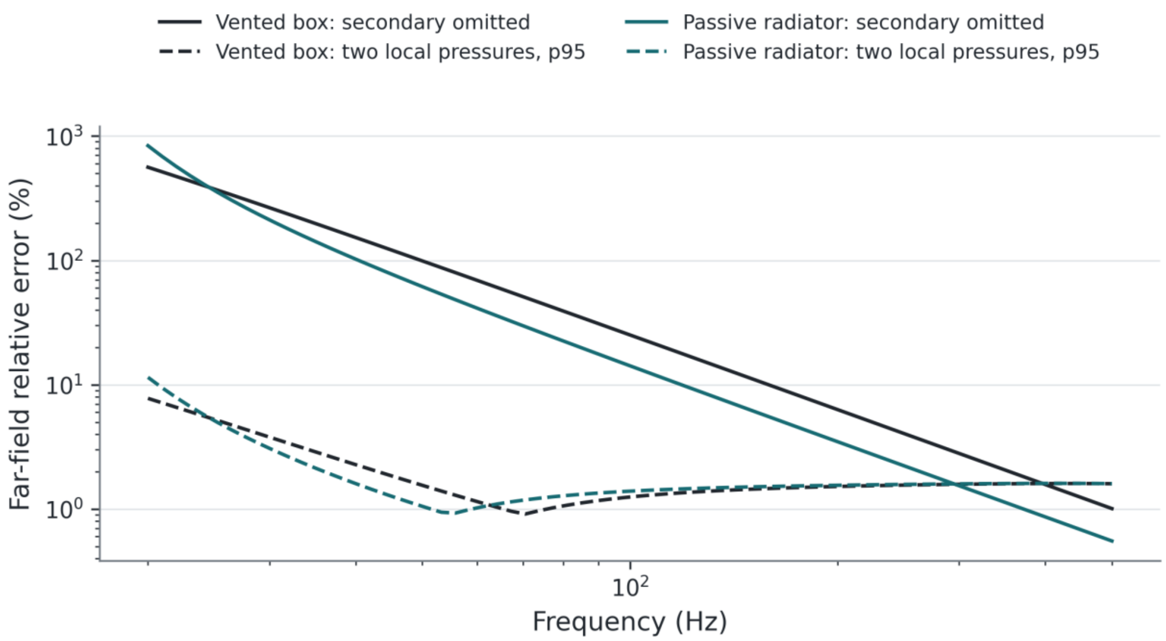

Figure 11. Secondary-radiator importance in the supplied vented-box and passive-radiator examples. Solid curves show far-field error when the secondary radiator is omitted; dashed curves show the 95th-percentile error with two registered local pressures in the declared synthetic model. These are different assumed systems, not measured tuning frequencies or errors of the real DUT. Backing data: extended 06_secondary_radiator.csv [4].

In the declared vented example, omitting the port near its 50.84 Hz response feature gives approximately 95.8% far-field error. A woofer-only local conversion is also strongly biased there. The point is not that every vented loudspeaker requires a permanent port microphone at every frequency. It is that material secondary radiation must be constrained by an adequate independent observation or a validated coupled model. A passive radiator can matter even though no current is supplied directly to it [4].

Electrical voltage, current and impedance are therefore valuable additional information. A calibrated back-EMF relation can constrain a coil-velocity state and can improve reference traceability. However, a terminal measurement does not uniquely determine arbitrary diaphragm rocking, breakup, cabinet vibration, waveguide radiation or an independently varying secondary source. For passive systems, an input measurement and a known crossover are not equivalent to direct access to every driver's terminal state.

The first practical source experiment should keep these alternatives open. A second available local channel can monitor a port or passive radiator where it contributes materially, or test a non-collinear mode on a sealed source. The choice should follow a source-class challenge and uncertainty analysis rather than the assumption that either "one channel is enough" or "every radiator always needs several sensors" [4].

16. Local geometric registration and nuisance control

Geometry changes the forward operator. A first-order expansion gives

$$\delta\mathbf{y} \simeq J_{\mathrm{g}}\delta\mathbf{g} + \mathbf{e}, \qquad \Sigma_{\mathrm{eff}} = \Sigma_e + J_{\mathrm{g}}\Sigma_{\mathrm{g}}J_{\mathrm{g}}^{\mathrm{T}} \tag{23}$$

in a real-stacked representation. Scanwise coordinate errors are correlated across all poses within a scan. Treating them as independent pressure noise understates their structure. The geometric Jacobian can also depend on the unknown source; a plug-in covariance is not automatically a globally valid uncertainty model [3,4].

The matched global comparison includes four complex source coefficients, two complex reflection coefficients, two plane offsets, two source-position parameters, twelve receiver radius/height coordinates, six scan gains, six scan phases and the speed of sound: 41 real parameters in total. Plane normals and source support remain restricted. The 98-variable conceptual inventory is broader and must not be confused with this finite numerical model [4].

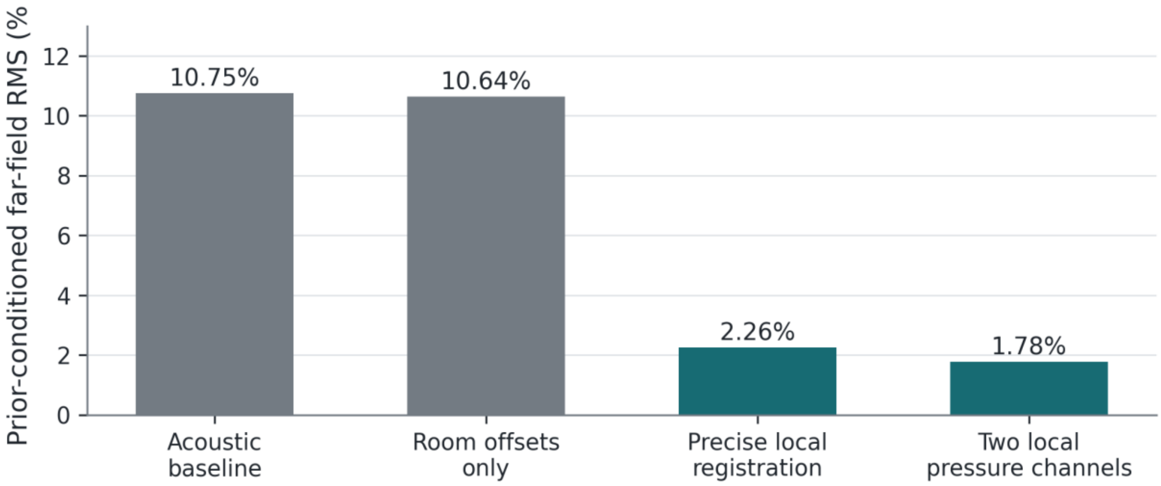

Figure 12. Value of registration in the matched 41-real-parameter model at 1 kHz. The acoustic baseline, room-offset observations, precise local registration and two local pressure observations give prior-conditioned target RMS values of approximately 10.75%, 10.64%, 2.26% and 1.78%. These are model-dependent uncertainties including stated nuisance priors, not measured real-DUT reconstruction errors or data-only certificates. Backing data: extended 04_global_prior_conditional.csv [4].

Figure 12 demonstrates a conditional but important result: local registration can be more valuable than improving only the room-plane offsets. The comparison does not show that room geometry is generally dispensable. The model already knows important parts of the scene, and the likelihood and prior contributions are explicitly separate. A new acoustic sensor whose complex gain is unconstrained may add another gauge, rather than supply the calibrated source information assumed in the comparison.

The earlier near-field study provides the necessary robustness boundary. In its richer 22-coefficient eccentric class, three local points per source group perform well with exact geometry but give approximately 397% median target error under the stated 15 mm far-receiver/0.5 mm near-field geometry stress. Covariance-aware weighting improves that result but does not pass the unchanged geometry criterion. The later restricted four-source/two-known-filter case is much better behaved, yet its 1 kHz two-local-channel manual-geometry tail is still about 47% [3,4].

These results are retained because omitting them would turn a conditional local-sensing success into a misleading robustness claim. They do not imply that every source class needs sub-millimetre surveying. They imply that the metrology requirement must be derived from the actual target, source class and uncertainty amplification. The same wavelength can correspond to very different inverse sensitivities.

Mechanical registration and acoustic-centre inference also have different meanings. A surveyed turntable axis, fiducial or probe transform constrains a physical datum. An effective acoustic phase centre can remain frequency dependent and model dependent. A geometric reference object should therefore calibrate the transformations it actually observes, not be described as measuring an acoustic source centre by itself [3–5].

17. Room reference scanning and geometric coverage

The proposed room scan is performed before the acoustic campaign, at a registered optical origin tied to the measurement frame. It can provide surface points, planes, normals, extents and visibility information. These quantities constrain reflection candidates and wave-domain geometry. They do not directly provide acoustic impedance, absorption, diffusion or a complex reflection coefficient [4,13,15].

A useful scan need not reproduce every small visual detail. It should describe surfaces that materially affect candidate early paths or low-frequency target-sensitive modes, with an uncertainty and visibility model. Conversely, a dense point cloud is not automatically complete: a sensor can sample many points on the same geometric subspace while missing floor, ceiling or out-of-plane orientation.

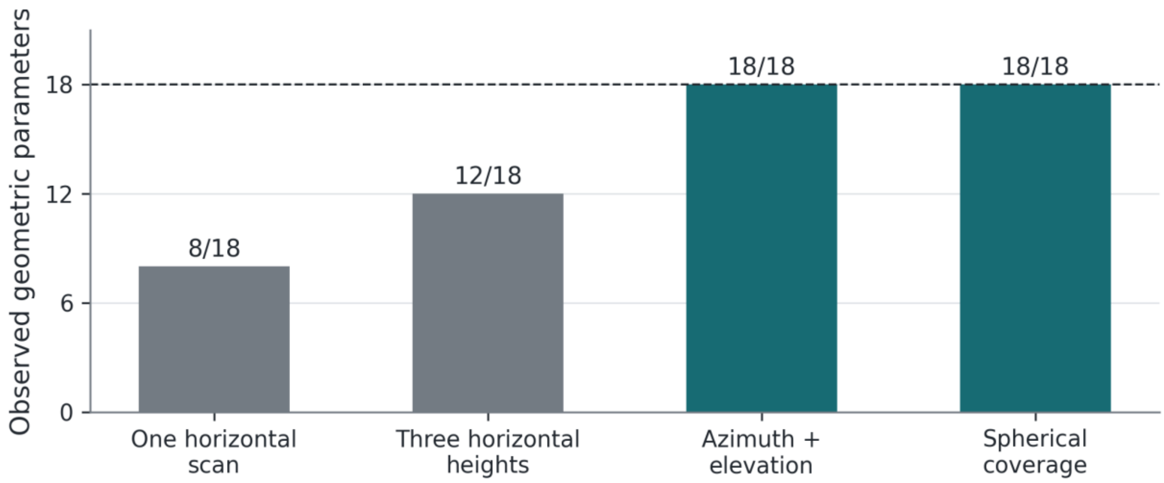

Figure 13. Geometric observability for six unconstrained planes, represented by 18 parameters. One horizontal scan observes eight parameters; three horizontal heights observe twelve; elevation-diverse and spherical designs observe eighteen in the synthetic model. The calculation assumes its declared scene and association conditions; it is not a real scanner's accuracy certificate. Backing data: extended 09_optical_geometry_rank.csv [4].

The rank comparison in Figure 13 explains why a single horizontal sweep is insufficient for a general three-dimensional room description. It can be adequate for a deliberately restricted map of vertical walls, but that restriction must come from an independent assumption or measurement. Several horizontal heights improve wall-normal information without automatically observing horizontal floor and ceiling surfaces. Elevation diversity, or separately registered observations of those boundaries, supplies different constraints [4].

The optical head can in principle rotate on a turntable or use its own scanning mechanism. Reusing the acoustic turntable is attractive only after calibrating the optical extrinsics, axis, encoder zero, tilt and runout. A nominal 5° acoustic sampling increment is not an optical pointing-accuracy specification. Similarly, placing a scanner at the future acoustic origin does not eliminate the optical-to-capsule transformation or guarantee optimal visibility.

A second optical view can expose occluded surfaces, but introduces another registration. The correct decision is target-driven: whether the additional surface information reduces relevant acoustic uncertainty enough to justify its transform and workflow burden. Scanner removal or retraction can reduce acoustic disturbance, provided the datum is retained and repeatability is measured. Neither an unspecified low-cost device nor an expensive metrology scanner is accepted without those checks [4].

18. Two-tier metrology and frequency-dependent geometry sensitivity

A useful provisional distinction is between broad room coverage and precise local registration. The room scan can prioritize major planes and candidate paths with moderate geometric detail. Local metrology can establish the source, turntable, receiver and sensor transforms more tightly where inverse sensitivity demands it. This can be more appropriate than demanding the same nominal accuracy everywhere, but a cost optimum has not been established [4].

For a plane with a fixed normal, an offset error δh moves the image source by $2\delta h$ along that normal. The reflected path change is bounded by $|\delta\ell| \leq 2|\delta h|$. Consequently a conservative single-path phase allowance $\phi_{\max}$ gives

$$|\delta\phi| \leq \frac{4\pi f}{c}|\delta h|, \qquad |\delta h| \leq \frac{c\phi_{\max}}{4\pi f}. \tag{24}$$

For a 10° phase allowance, the offset scales are about 47.6 mm at 100 Hz, 4.76 mm at 1 kHz and 0.476 mm at 10 kHz. They are single-path kinematic bounds. They omit normal error, registration, source uncertainty, boundary filtering and the conditioning of the inverse. A small path error can be amplified, while an unknown reflection coefficient can absorb some phase variation at the cost of identifiability [4].

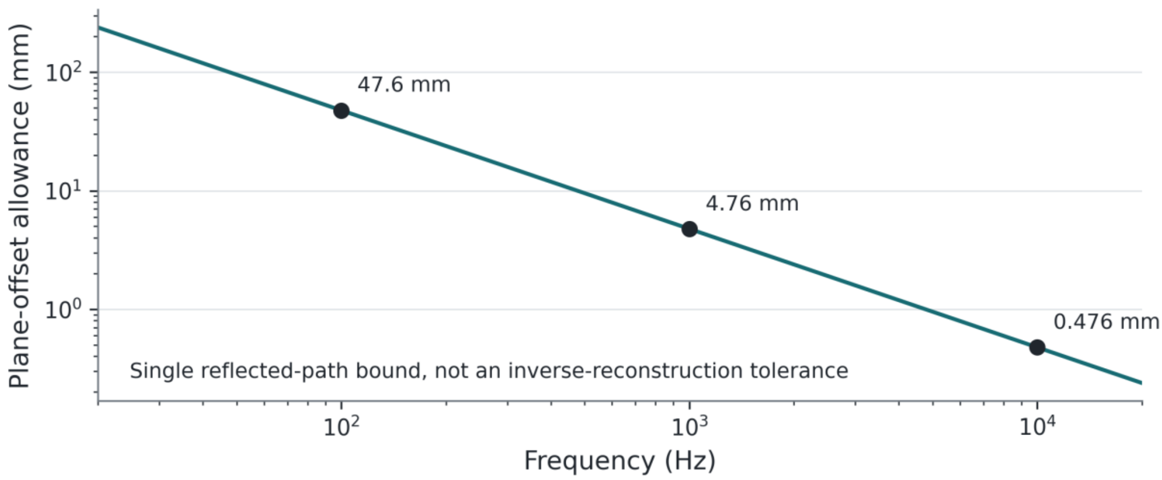

Figure 14. Conservative plane-offset allowance for a 10° single-reflection phase budget. The inverse-frequency relation motivates different geometric requirements by target and band. It does not specify a universal scanner accuracy or establish complete reconstruction robustness. The supplied values use $c = 343$ m/s. Backing data: extended 10_plane_phase_budget.csv [4].

Low frequency does not make room geometry irrelevant. The converged smooth-source, damped rectangular-room calculation gives approximately 17.7% field change near 31.18 Hz when a room dimension is perturbed by 20 mm. At 20 Hz the corresponding change is much smaller. The resonance sensitivity depends on source overlap, receiver position and loss, so this example must not be treated as a measured room specification. It establishes why a simple “long wavelength permits coarse geometry” rule is incomplete [4].

Local geometric observability also needs a parameter count. Two scalar range observations cannot determine an arbitrary six-degree-of-freedom pose without additional constraints. A symmetric reference artifact can leave axial or rotational freedoms unobserved. Multiple registered fiducials or constrained fixture geometry may supply the missing datum, but the uncertainty belongs to the complete chain from optical point to acoustic capsule and source support.

The engineering objective is selective precision. A low-cost room scanner may be adequate for geometric candidate generation if its range bias, coverage, pointing and registration are qualified. Tighter local sensing may be justified for source/probe transforms. Neither conclusion follows from advertised resolution alone, and no component selection or final optical architecture is frozen by the present analysis.

19. Geometry-constrained reflections and a hybrid room model

For a candidate plane $\mathbf{n}_j^\top \mathbf{x} = h_j$ with unit normal $\mathbf{n}_j$, the image of a source position $\mathbf{s}$ is

$$\mathbf{s'}_j = \mathbf{s} + 2\left(h_j - \mathbf{n}_j^\top \mathbf{s}\right)\mathbf{n}_j, \qquad \tau_j = \frac{\|\mathbf{x} - \mathbf{s'}_j\|}{c}. \tag{25}$$

For the rotating DUT, $\mathbf{s}$ and its modal orientation follow the known pose and eccentricity. An image operator must transform directional radiation consistently; replacing a directional source by an omnidirectional amplitude with only a corrected distance would change the model. Independent source-image and receiver-image constructions are valuable implementation checks [3,4,12].

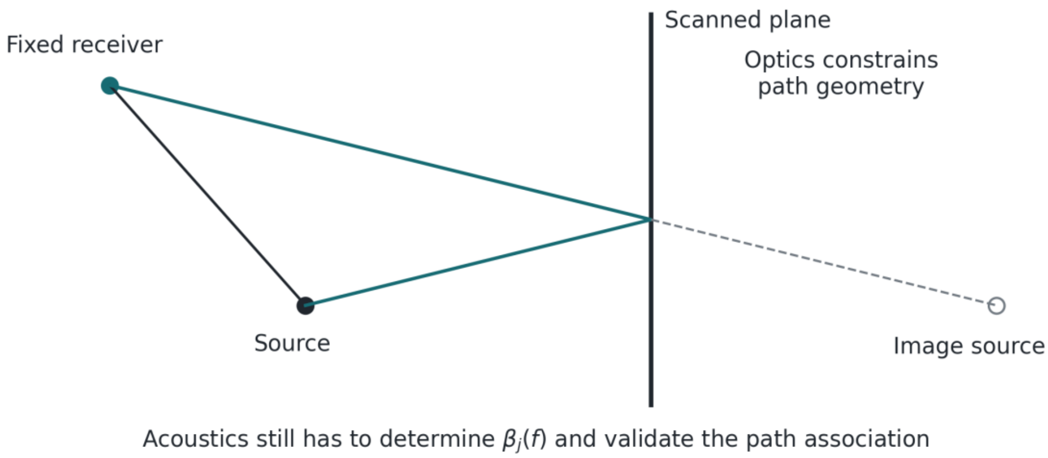

Figure 15. Geometry-constrained reflection candidate. A scanned plane constrains path length and direction, while acoustic measurements must estimate the complex response and validate its association. The diagram is schematic and omits finite extent, occlusion, diffraction and source directivity; those effects remain explicit modelling or discrepancy terms [4,12,13].

A planar identity useful for checking geometry is

$$\ell_\mathrm{r}^2 - \ell_\mathrm{d}^2 = 4\left(h - \mathbf{n}^\top \mathbf{x}\right)\left(h - \mathbf{n}^\top \mathbf{s}\right). \tag{26}$$

The factorization provides a coherent receiver–pose signature under the stated one-plane hypothesis. It does not identify a real wall unless the associated acoustic events actually belong to that path. Echo sorting is a substantive inverse problem: different receivers can receive reflections in different orders, and some detected peaks do not correspond to first-order wall echoes. Published room-shape reconstruction exploits geometric consistency to address that association problem [13].

The proposed room model is source linked:

$$p_{\mathrm{r}}(f) = \sum_{j} \beta_j(f) E_j(f; \mathbf{g}) \mathbf{a}(f) + p_{\mathrm{res}}(f). \tag{27}$$

Optics constrains E_j through geometry. Acoustics estimates β_j and tests path consistency. A restricted residual accounts for effects not represented by the selected paths; its overlap with source signatures must be assessed. Allowing an arbitrary new complex coefficient at every sample would defeat the purpose of the geometric constraints.

Finite source-linked reflection models in the supplied research recover known synthetic components and permit joint coefficient estimation with variable projection. Those tests assume their source support and candidate geometry. The richer-truth checks show that omitted compound reflections or inaccurate association can bias the direct-field target even when the fit improves. A general causal, multi-band boundary-impedance and overlapping-waveform inverse for the actual room is still open [4].

For lower-frequency room behaviour, a modal or full-wave model can exploit scanned geometry without relying on a sparse specular-path approximation. A generic modal response contains terms proportional to $\psi_\nu(\mathbf{x}) s_\nu / (\omega_\nu^2 - \omega^2 + i2\zeta_\nu \omega_\nu \omega)$, where geometry determines mode shapes and frequencies, while damping and source coupling remain acoustic parameters. This separates geometric knowledge from material loss rather than pretending the point cloud is acoustic ground truth. Boundary-informed Bayesian reconstruction is a relevant complementary formulation, but its prior assumptions and experimental scope are not transferred as PHYSICAL LAB acceptance criteria [4,15].

20. Real development data and the restricted Normal Model

The real-data result that can presently be stated positively is accurate angular prediction of total complex pressure at already observed receiver configurations. The preserved full-IR data are mapped to six receivers, 72 unique poses and nine native frequency bins near 500–1500 Hz. A deterministic nested procedure fits candidate Fourier orders on one angle set, selects order on a disjoint calibration set, refits on their union and evaluates withheld angles [3,4].

The 54 receiver/frequency errors have median 0.0146670 and 90th percentile 0.0233363: approximately 1.47% and 2.33% relative complex amplitude error. These are development folds on previously inspected data, not fresh blind validation. Their significance is useful interpolation of the measured process with explicit data identity and reproducibility.

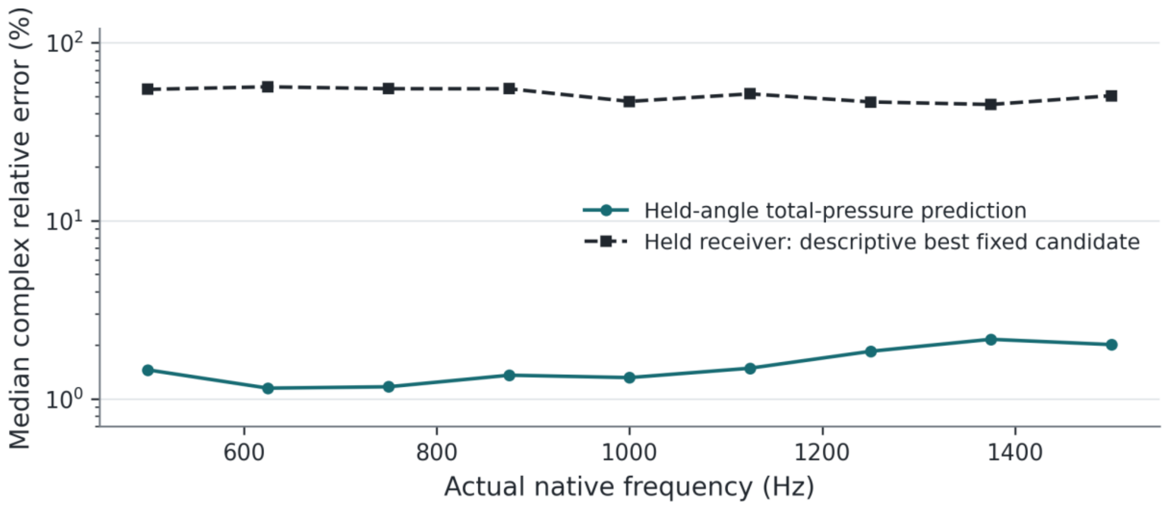

Figure 16. Different real-development targets have very different errors. Held-angle total-pressure prediction is accurate at the observed receiver configurations. The descriptively best fixed candidate in a separate whole-receiver extrapolation comparison remains inaccurate. The plotted curves are per-frequency medians, not pooled median/p90 values. Good angular interpolation is not a separated-component reference. Backing data: Phase-II 11_real_prediction_boundary.csv [3,4].

The whole-receiver study separately withholds every physical configuration. Among its tested finite hypotheses, the descriptively best fixed combination has pooled median error about 51.5% and p90 about 66.6%. "Best" is a post-hoc description of that candidate set, not an independently selected-model validation. The result does not prove that every richer source-linked multipath model must fail. It does show that the tested models and existing manual geometry do not qualify physical extrapolation [3].

These distinctions motivate separate Normal Model modes. The supported prediction mode represents total pressure versus angle and includes room effects in its target. A conditional physical mode requires a validated source representation, registered geometry, a common complex reference, a constrained room model and bounded discrepancy. A gated mode requires a qualified window error. A hybrid output is permitted only when its inputs estimate the same target and satisfy their own validity conditions [3,4].

The current corpus contains no actual co-rotating local source data, verified room-scan planes, independent p–u/LDV reference or separated-component truth for this DUT. The source-assisted results remain synthetic evidence. A new experimental campaign must establish these observations rather than silently treating the proposed fixture or scanner as already present. In particular, a new precise survey cannot retroactively prove the old manual receiver positions.

21. Proposed reconstruction workflow and data contract

The proposed system should retain a common geometry and evidence model from acquisition through output. A measurement record needs the complex quantity, frequency, physical receiver identity, DUT pose, reference and calibration, rather than only a nominal polar angle. An optical observation needs its origin, extrinsics, uncertainty and scene interpretation. A local pressure or electrical observation needs an explicit source-state relationship and contamination allowance [1,3,4].

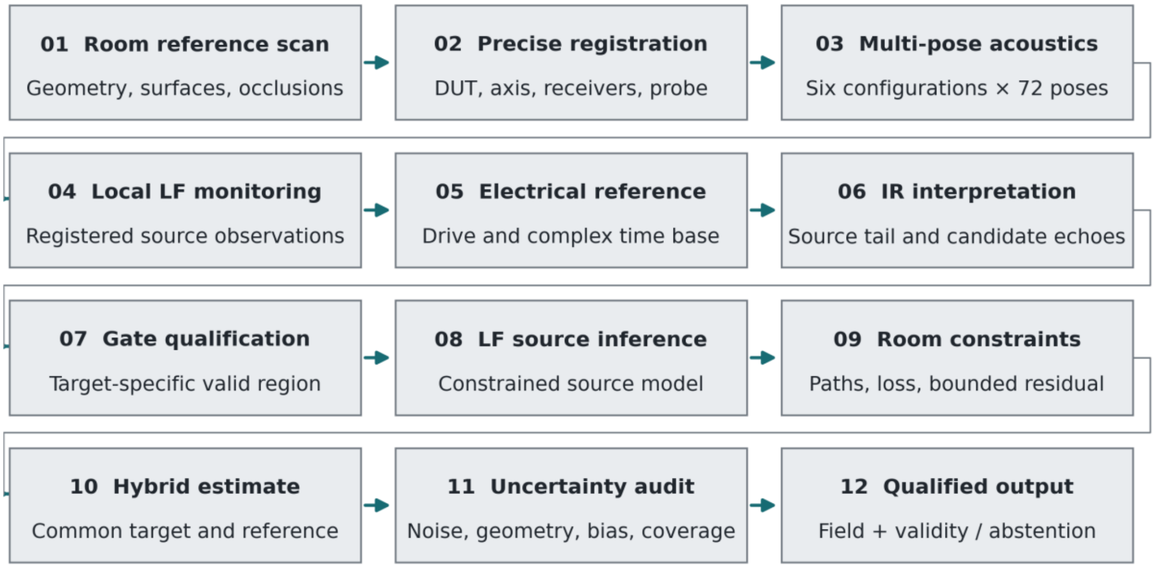

Figure 17. Proposed complete workflow. The twelve stages describe logical dependencies, not twelve isolated sequential acquisitions: local LF monitoring and electrical referencing should be synchronized with the pose measurements where implemented. Geometry and source-state information constrain the inverse; gate qualification and uncertainty determine whether a hybrid target can be issued. This is a future workflow, not a claim that all modules are physically validated [4].

A practical sequence starts by registering the optical and acoustic datums, identifying relevant surfaces, and checking the repeatability of the source/reference state. The acoustic campaign then acquires the multi-pose field together with the selected local LF and electrical observations. IR analysis proposes source and reflection structures, while the optical model supplies candidate paths with uncertainty. Source-class and room-class checks should precede interpreting a fitted component as physical.

For the source-assisted calculation, form the joint observation operator and covariance from the retained pressure, local and reference measurements. Assess data-only rank, target-changing nulls and near-null amplification before selecting a regularizer. Fit acoustic boundary parameters within the restricted source-linked model, and challenge the result on held-out receiver/pose/frequency observations appropriate to the target. A numerical optimizer's convergence is an algorithmic condition, not the final validity gate.

The gating module must preserve the ungated response, the applied window and its qualification evidence. Before merging, its estimate must be expressed at the same coordinate, distance, directional target and phase reference as the inverse estimate. A simple $1/r$ normalization is not a general near-to-far transformation for a multimode source. Geometric display correction and physical forward-model correction must not be applied twice.

The output should include the estimated complex field, the supported source and room class, the data provenance, frequency-dependent uncertainty and a validity state. A missing band should remain explicitly unavailable when its error is not bounded. Analyzer-independent software is a future integration objective: its core should consume a stable scientific data contract rather than depend on one instrument's display units or export conventions. The present programme does not claim that every acquisition backend or future product module is implemented [3,4].

22. Hybrid estimation with covariance, correlation and bias

Let $\hat{z}_{\mathrm{L}}$ and $\hat{z}_{\mathrm{H}}$ estimate the same complex target using source-assisted inversion and qualified gating. For a real weight $w \in [0,1]$, define

$$\hat{z} = w\hat{z}_{\mathrm{L}} + (1-w)\hat{z}_{\mathrm{H}}. \tag{28}$$

A smooth-looking blend is not enough. The two estimates can share the same pressure noise, calibration reference or geometry error. Their cross-covariance must therefore be included. For scalar mean-square variance terms v_{L} and v_{H}, real cross-covariance contribution c_{LH}, and nonnegative coherent bias bounds b_{L} and b_{H}, the supplied risk model is

$$\mathcal{R}(w) = w^2 v_{\mathrm{L}} + (1-w)^2 v_{\mathrm{H}} + 2w(1-w)c_{\mathrm{LH}} + [w b_{\mathrm{L}} + (1-w) b_{\mathrm{H}}]^2. \tag{29}$$

The last term bounds coherently aligned biases. It is not a claim that unknown deterministic biases are independent random noise. Differentiating this quadratic gives, for a positive denominator,

$$w_{\mathrm{opt}} = \mathrm{clip}_{[0,1]}\left[\frac{v_{\mathrm{H}} - c_{\mathrm{LH}} + b_{\mathrm{H}}^2 - b_{\mathrm{L}} b_{\mathrm{H}}}{v_{\mathrm{L}} + v_{\mathrm{H}} - 2c_{\mathrm{LH}} + (b_{\mathrm{L}} - b_{\mathrm{H}})^2}\right]. \tag{30}$$

A degenerate denominator needs a declared fallback; invalid covariance or unqualified input identity requires abstention rather than a numerical default. For a vector directional target, variance terms can be formed from a declared weighted trace or another explicit scalar objective. A matrix-valued fusion can be investigated, but should not be substituted without revisiting reference, correlation and bias assumptions [4].

The supplied merge implementation exercises those boundaries on synthetic inputs. A separate example using known synthetic gate error to determine weights is explicitly an oracle diagnostic. It is not a real-data model-discrepancy estimator. The existence of the weighting formula therefore does not close the difficult experimental problem of qualifying b_{L} and b_{H} for the actual loudspeaker.

Frequency smoothing of weights may reduce an undesirable abrupt transition, but can increase the local risk relative to the independently optimal weight. The smoothed result must be reassessed. Magnitude, complex phase, group delay and directional patterns should all remain consistent with the declared target. A crossfade cannot repair a normalization reference near zero, an invalid propagation model or incompatible source states.

This framework also explains why no universal transition frequency is specified. A long-lived source mode may make the gating bias large where the inverse is otherwise well conditioned; a source-mode or room-model mismatch may make the inverse bias large elsewhere. The selected method should follow qualified risk, and a gap in qualification should remain a gap. The present real-DUT crossover fields remain unassigned [4].

23. Uncertainty, confidence and independent observables

The final uncertainty budget should distinguish acoustic noise, complex channel calibration, timing, receiver placement, source-reference location, turntable geometry, local-sensor coordinates, room surfaces, boundary response, source model and discrepancy. Some contributions are correlated, some are bounded systematic terms, and some are unresolved model alternatives. Combining them into a single fitted residual would conceal the information needed for a scientific decision [3,4].

On an observable subspace, a first-order target perturbation can be bounded in the form

$$\|\delta \mathbf{z}\| \lesssim \|B A_w^{\dagger}\| (\|W\mathbf{e}\| + \|W\boldsymbol{\delta}_{\mathrm{model}}\| + \|W\delta A\,\mathbf{q}\|) + \|\delta B\,\mathbf{q}\|, \tag{31}$$

where $A_w = WA$, the dagger denotes the Moore–Penrose inverse, and the target's own geometric variation is retained in δB. This is a local bound under an adequate state norm and validity domain. It does not give finite data-only uncertainty when a target-changing null direction or unbounded discrepancy remains. A Bayesian posterior can incorporate justified prior information, but a narrow prior-driven posterior is not experimental validation.

Independent velocity or surface-motion observations can probe different missing directions. In a homogeneous source-free fluid,

$$\mathbf{u} = -\frac{\nabla p}{i\omega\rho_0}. \tag{32}$$

The equation predicts what an independently measured particle-velocity channel would observe. It does not make a gradient calculated from existing pressure samples an independent measurement. For an injective transformation $\mathbf{z} = T\mathbf{y}$ of retained data with nonsingular original covariance,

$$A^{\mathrm{H}}T^{\mathrm{H}}\left(T\Sigma T^{\mathrm{H}}\right)^{\dagger}TA = A^{\mathrm{H}}\Sigma^{-1}A. \tag{33}$$

Thus pressure and a derived difference must retain their joint, potentially singular covariance. Treating the derived quantity as a new independent channel double-counts information. Genuine additional pressure positions can help because they add observations; differencing those positions is a choice of representation [2–4].

Published pressure–velocity separation demonstrates why true velocity is a relevant independent sensing route [9,10]. Surface velocity measured optically is different again: LDV observes motion along its optical sensitivity direction, which must be related to the surface-normal state required by the acoustic model [19]. The prescribed-disk study supports spatially distributed sensing, not the superiority of a single central LDV point or a universal need for a p–u probe.

A future confidence system should separate evidence and numerical quality. *Validated* should require an accepted physical reference and uncertainty statement for the declared scope. *Conditional* can identify an observable restricted model with qualified assumptions. *Low confidence* can flag large but bounded target uncertainty. *ABSTAIN* is appropriate for unobservable targets, incompatible references, invalid domains or unbounded discrepancy. These are proposed output semantics, not current measurement certificates.

24. Practical architectures, verification and research roadmap

The strongest provisional implementation is a small registered LF source-signature experiment, not an immediate dense array or a premium full-room scanner. It should provide one local channel near the lowest relevant active radiator and a second available channel for a material port/passive radiator or a non-collinear source-mode challenge. Additional fixed mounting positions allow the source class to be tested without asserting that all positions become permanent product sensors [4].

Table 4. Provisional architecture levels and acceptance boundary.

Architecture	Purpose	Required evidence before physical claims
Existing-data prediction	Total-pressure angular interpolation	Data identity, repeatability and withheld-angle error
Registered source-assisted research fixture	Test one/two local LF observations with a common reference	Source-class adequacy, actual coordinate/calibration budget, secondary radiation
Room-aware hybrid prototype	Add elevation-diverse geometry and qualified gating	Acoustic/optical registration, path validation, bias-qualified common targets
Advanced benchmark	Independent p–u or distributed LDV and tighter metrology	Modality calibration, matching observable definition, loading/scattering checks
Future practical system	Use only additions justified by target improvement	Independent physical truth, reproducibility and a validated operating domain

The fixture should retain a far/reference observation and a common electrical/phase reference. It should withhold spatial and pose observations that distinguish scalar source behaviour from relevant higher modes. The first decision is whether the low-dimensional source signature transfers within the *measured* uncertainty budget. Only after that should the programme qualify source-linked room reconstruction and the gated target against independent component or direct-field evidence.

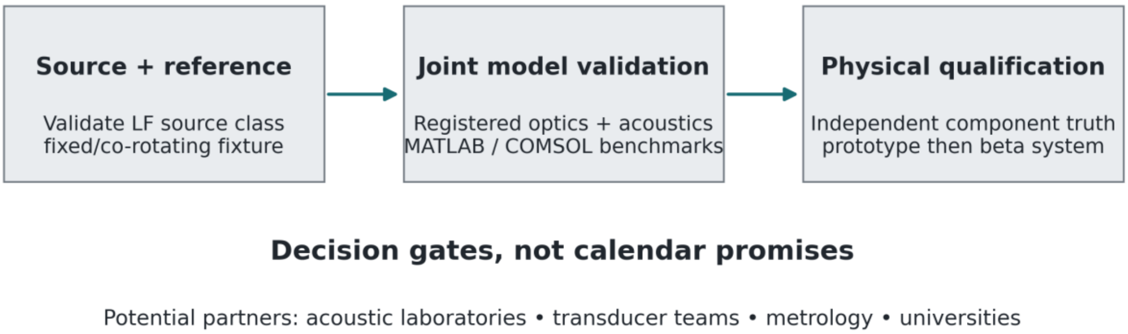

Figure 18. Research roadmap as evidence-dependent milestones. Source/reference validation precedes joint model qualification, which precedes physical component acceptance and a practical prototype. There is no invented schedule, fixed sensor count or commercial release claim. Academic, industrial and metrology partners can contribute at different validation stages [3,4].

Independent computation remains important. The supplied Python campaigns include analytic controls, synthetic cases, saved operators and witnesses, and real-development replay. The earlier V3.63p MATLAB harness passed 52/52 checks on the recorded local installation. The later Phase-II and extended MATLAB harnesses still require execution; an earlier pass cannot validate modified mathematics or code [3,4,6].

The COMSOL programme is prepared as a controlled forward-model check, not claimed executed. It should begin with analytic Green, piston and prescribed-mode cases, then add actual sensor geometry, simple reflecting boundaries, source–structure coupling and selected low-frequency room configurations. At least three refinement levels, domain/PML checks where applicable, solver tolerance checks and matched source/loss conventions are required. The supplied plan's prospective 1% forward comparison and 0.5% final-refinement criteria are distinct from floating-point identity tests [4,17].

Physical validation must then address real source-mode complexity, secondary-radiator interactions, probe loading, calibration drift, optical-to-acoustic registration, path association and source/room back-action. An anechoic, sufficiently controlled outdoor or other defensible physical reference may be used within its own uncertainty and target definition. A time gate from the same unqualified room data is not independent truth. The reference strategy should be chosen to test the intended product claim, including whether it is an outgoing support-defined estimate or an unchanged-drive counterfactual.

25. Industrial relevance, collaboration and conclusions

25.1 Potential use in development workflows

The potential industrial value is access to richer and more traceable loudspeaker radiation information when a full-size anechoic environment is unavailable or impractical. Loudspeaker and studio-monitor development could benefit from qualified directivity and driver-integration data. Professional audio and sound-reinforcement teams could use declared virtual receiver targets and low-frequency source diagnostics. Transducer, waveguide and crossover teams could compare prototypes in a common representation linked to their simulation models. These are prospective applications, not claims of existing customer adoption or demonstrated cost savings.

Automotive and consumer-audio development present related opportunities for component characterization and simulation correlation. Transfer to a vehicle installation or a compact integrated product would require a corresponding source/support and boundary model; the present six-configuration loudspeaker study does not validate those different environments. R&D laboratories, universities and acoustic consultants could also use the observability tools to design more informative experiments and to distinguish prediction performance from physical interpretation.

For measurement-system suppliers, the longer-term opportunity is an analyzer-independent reconstruction layer with explicit acquisition geometry, reference semantics and confidence outputs. For industrial vibroacoustics, source-state information and inverse acoustic continuation may be useful beyond loudspeakers, but the radiator physics and target must be redefined. The programme's value proposition is therefore not a universal room-removal button. It is a framework for determining which measurements can support a particular field claim, at which frequencies, and with what uncertainty.

Workflow automation can have scientific value by reducing manual placement, time-reference mismatch and drift. Its benefit must still be measured. The existing research does not supply a validated acquisition-time reduction, a complete bill of materials or a procurement optimum. A future practical system should choose the least complex architecture that reproduces the qualified target, rather than adding sensors merely to increase nominal channel count [3,4].

25.2 Collaboration and research support

PHYSICAL LAB welcomes discussions with industrial and academic partners interested in experimental validation, prototype development, measurement campaigns and potentially jointly funded R&D. Relevant contributions include access to characterized radiators, independent acoustic reference facilities, calibrated multichannel acquisition, optical registration, p–u or LDV benchmarks, and full-wave source/probe models.

Suitable public or private research-support opportunities, innovation grants and collaborative funding programmes are welcome where they accelerate physical validation and prototype development. No funding award, consortium participation or industrial adoption is implied. The most useful near-term collaboration is a well-defined experiment that reduces a specific uncertainty in the source class, reference chain, geometric registration or physical target, with agreed acceptance criteria and data provenance.

25.3 Scientific conclusion

The research establishes a coherent set of mathematical and numerical lessons. The stationary six-ring control contains a target-changing nullspace. Correct pose modelling introduces shared-source structure and separates rotational from eccentric-path information, but full finite rank does not ensure robustness. Local observations can constrain or stabilize source directions that room pressures observe weakly, while their required number depends on source complexity. Co-rotation improves repeatability without eliminating constant room contamination. Room scans constrain geometry and candidate paths, but not acoustic boundary response. Qualified gating must bound both discarded direct dynamics and retained reflections [2–5].

These findings support a registered, target-aware, frequency-dependent hybrid architecture. Limited LF source assistance, geometry-constrained room operators and a qualified time-window estimate can contribute different pieces of information. Their combination is justified only when the estimands, references, covariance and bias bounds are compatible. A smooth blend cannot supply missing physical information.

The immediately supported real-data capability remains total-pressure angular prediction at observed receiver configurations. Real free-field continuation and source/room attribution are not physically certified. The next research stage is a small fixed/co-rotating source-class experiment with measured registration and references, followed by optical/acoustic path qualification and an independent component-truth comparison. This is a concrete route to determining the minimum practical architecture, without pretending that a universal count or crossover frequency is already known.

Success would mean useful directional or free-field data from a practical in-room measurement, with a traceable reference, quantified uncertainty and explicit validity limits. That goal is more demanding than a visually corrected response, and more valuable than an unconditional number without an information basis. Product V3.63 remains frozen; no V3.64 or final hardware architecture is promoted by this publication. Physical component claims remain **ABSTAIN** until their independent validation requirements are met.

Appendix A. Mathematical checks and interpretation details

A.1 Complete Cauchy data versus finite pressure traces

On a complete sphere with independently available pressure and normal derivative, each angular mode has two radial equations. For the outgoing/regular pair, the radial matrix is $\begin{bmatrix} h_l^{(2)}(kR) & j_l(kR) \\ kh_l^{(2)\prime}(kR) & kj_l{}'(kR) \end{bmatrix}$. Its determinant is $i/(kR^2)$ by the spherical Bessel Wronskian [8]. This nonzero determinant removes the two-pressure radial resonance for an already observed angular mode. It does not establish angular completeness from six pressure rings or from a few local velocity samples.

The distinction is important for p–u comparisons. An independently measured velocity adds a physical observable. A finite difference of the same stored pressures does not. Additional pressure locations can approximate a derivative with a known finite-difference error and covariance, but that is still information supplied by the additional locations. Closed-surface identities, finite modal truncation and sparse measurement operators have different prerequisites [2,3,9,10].

A.2 A verification chain for a claimed target

A target claim should retain the physical model, source domain, coordinate convention, row ordering and complex reference. The unregularized operator must be reconstructed from those definitions. Whitening and coefficient scaling must be recorded so that another implementation can reproduce its singular spectrum and nullspace in the same metric. For each saved null vector, both the acquisition residual and target response must be evaluated. For an added modality, the same missing-space basis must be used rather than a more favourable unrelated control.

A robust result then requires perturbations in the operator as well as the right-hand side. Geometry, source and room drift can be coherent; common calibration does not behave like independent noise. Model discrepancy must be challenged by richer truth or independent physical observations. An exact in-basis synthetic reconstruction tests implementation and conditional identifiability, while a held-out physical target tests the claimed operating domain. Neither should be relabelled as the other [2–4].

A.3 Reference-dependent normalized targets

For a translated source, the far-field amplitude acquires a factor $e^{+ik\hat{\mathbf{u}}^{\top}\delta\mathbf{t}}$ in the chosen phasor convention. A normalized complex ratio therefore changes by $e^{+ik(\hat{\mathbf{u}}-\hat{\mathbf{u}}_0)^{\top}\delta\mathbf{t}}$; its magnitude is unchanged. This explains why a missing coordinate datum can be harmless for one target and relevant for another. It does not make phase-insensitive directivity immune to source-model mismatch or room ambiguity.

The derivative of a normalized magnitude is undefined at an exact zero in the elementary quotient representation. A practical implementation needs an explicit reference floor and a target-specific treatment of directional zeros. Replacing those regions by arbitrarily smooth values conceals uncertainty. Local Jacobian conclusions should always be identified as local and should not be promoted into global uniqueness without further analysis [3,4].

Appendix B. Reproducibility, publication scope and limitations

This manuscript is a publication synthesis of the supplied research state. It does not claim a new full execution of every historical scientific campaign. Selected numerical figures are regenerated from the supplied machine-readable backing data; Figure 5 is an explicitly labelled rigid-geometry illustration. Schematics describe analytical relationships or proposed workflows. No plotted response is invented as an experimental measurement.

The publication figure workbook includes the plotted data, provenance and evidence classifications. CSV files retain the supplied values; SVG and PDF figure files support vector reuse; PNG versions provide high-resolution Word compatibility. The editable Word manuscript contains native mathematical objects, editable text, captions and references. Its PDF is rendered from that same document. The LinkedIn carousel is a separate communication narrative, not a compressed page-by-page version of the paper.

The evidence ledger distinguishes analytic statements, conditional numerical results, real-development observations and proposals. The latest extended campaign's 40 regression methods and 250 saved-evidence checks are inherited scoped verification results, not 290 independent experiments and not tests rerun by publishing this manuscript. Similarly, the historical 52/52 V3.63p MATLAB pass is not reassigned to the unexecuted later harnesses. COMSOL and new physical source/room truth are still absent [3,4,6].

Unresolved scientific work includes the actual source/support and crossover inventory; fixed/co-rotating local sensing; complex channel and optical calibration; real path association with overlapping source waveforms; causal boundary modelling where required; source/back-action transfer; independent MATLAB and full-wave comparisons; and physical target-error qualification. The supplied numerical evidence motivates these experiments but does not replace them.

The publication does not modify production code, use a reserved blind-validation seed, freeze sensor count or select a final bill of materials. Potential applications and collaboration statements are forward-looking. No publication venue, peer-review acceptance, grant award, commercial readiness or customer adoption is asserted.

References

[1] PHYSICAL LAB. *Frozen Acquisition Contract V2: operator-confirmed protocol*. 14 September 2026. Private project record, PHYSICAL_LAB_SFS_ACQUISITION_CONTRACT_V2_FROZEN_2026-09-14.json. Complete supplied source; six room-fixed configurations, rotating DUT, nominal geometry and declared unknowns.

[2] PHYSICAL LAB. *Sound-Field Separation: Scientific Due Diligence and Research Reconstruction*. Phase-I scientific report, checkpoint, handoff and research-source package, September 2026. Private complete report and numerical evidence, PHYSICAL_LAB_SFS_GPT6_PRO_SCIENTIFIC_REPORT.pdf and accompanying archive.

[3] PHYSICAL LAB. *SFS: Multi-pose observability and near-field source-state reconstruction*. Phase-II final report, 31 pages, September 2026. Private complete source and result corpus, PHYSICAL_LAB_SFS_PHASE2_FINAL_REPORT.pdf and PHYSICAL_LAB_SFS_PHASE2_RESEARCH_SOURCE.zip. Specific CSV/JSON records are identified in captions and the publication data ledger.

[4] PHYSICAL LAB. *Extended free-field, source-state, room-geometry and hybrid reconstruction study*. Extended scientific report, 37 pages, September 2026. Private complete checkpoint, handoff and numerical corpus, PHYSICAL_LAB_SFS_EXTENDED_FREEFIELD_REPORT.pdf and PHYSICAL_LAB_SFS_EXTENDED_RESEARCH_SOURCE.zip. Current project-state authority for this synthesis.

[5] PHYSICAL LAB. *3-Plane / 2-Radius Real Measurement Qualification V1*. 14 September 2026. Private checkpoint, PHYSICAL_LAB_SFS_CHECKPOINT_3PLANE_2RADIUS_REAL_MEASUREMENT_V1_2026-09-14.md. Timing-derived acoustic reference, geometry uncertainty and revision of the earlier single-polar estimate.

[6] PHYSICAL LAB. *V3.63p local MATLAB parity handoff*. 14 September 2026. Private machine-readable record, SFS_LATEST_HANDOFF(20260914-030011).json. Records 52/52 checks on MATLAB R2025b Update 2 for that historical harness; not later-code acceptance.

[7] Maynard, J. D., Williams, E. G., and Lee, Y. "Nearfield acoustic holography: I. Theory of generalized holography and the development of NAH." *Journal of the Acoustical Society of America* 78(4), 1395–1413 (1985). DOI: 10.1121/1.392911. Primary bibliographic/abstract record checked through NASA NTRS; full article not re-audited for this publication.

[8] NIST. *Digital Library of Mathematical Functions*, §14.30, Spherical and Spheroidal Harmonics, and §10.50, Wronskians and Cross-Products. Official definitions and identities, accessed 15 September 2026. Convention reference, not an external proof of the PHYSICAL LAB ranks.

[9] Ma, F., Zhang, W., and Abhayapala, T. D. "Real-time separation of non-stationary sound fields on spheres." arXiv:1901.05122 (2019). Primary author abstract and metadata reviewed; spherical pressure/radial-velocity formulation. No claim of reproducing its complete implementation.

[10] Fernandez-Grande, E., Jacobsen, F., and Leclère, Q. "Sound field separation with sound pressure and particle velocity measurements." *Journal of the Acoustical Society of America* 132(6), 3818–3825 (2012). DOI: 10.1121/1.4763988. Primary abstract and metadata reviewed; device-specific performance is not imported as a noise budget.

[11] Fernandez-Grande, E., Xenaki, A., and Gerstoft, P. "A sparse equivalent source method for near-field acoustic holography." *Journal of the Acoustical Society of America* 141(1), 532 (2017). DOI: 10.1121/1.4974047. Primary abstract and metadata reviewed; sparse representation and coherence context.

[12] Allen, J. B., and Berkley, D. A. "Image method for efficiently simulating small-room acoustics." *Journal of the Acoustical Society of America* 65(4), 943–950 (1979). DOI: 10.1121/1.382599. Full author/institution-hosted paper consulted; not a validation of a two-path approximation to the actual room.

[13] Dokmanić, I., Parhizkar, R., Walther, A., Lu, Y. M., and Vetterli, M. "Acoustic echoes reveal room shape." *Proceedings of the National Academy of Sciences* 110(30), 12186–12191 (2013). DOI: 10.1073/pnas.1221464110. Full open primary text reviewed; geometry and echo-association assumptions remain explicit.

[14] Bi, C.-X., and Bolton, J. S. "An equivalent source technique for recovering the free sound field in a noisy environment." *Journal of the Acoustical Society of America* 131(2), 1260–1270 (2012). DOI: 10.1121/1.3675004. Primary abstract reviewed; distinguishes outgoing/scattered contributions from the desired free field.

[15] Sundström, D., Elvander, F., and Jakobsson, A. "Boundary-Informed Sound Field Reconstruction." arXiv:2506.13279 (2025). Full v1 HTML preprint consulted. Bayesian boundary geometry/impedance prior; preprint status retained, and its numerical tolerances are not adopted as current-project specifications.

[16] Ishikawa, K., Tanigawa, R., and Harada, N. "Differentiable equivalent source method: Joint optimization of equivalent source positions and strengths with implicit geometry constraints." *JASA Express Letters* 6(5), 050001 (2026). DOI: 10.1121/10.0043709. Primary open article and metadata checked; contextual candidate method, not implemented or validated here.

[17] COMSOL. *Baffled Piston Radiation*. Official tutorial-model description, accessed 15 September 2026. Canonical model/analytic comparison reference. No COMSOL execution is claimed by this manuscript.

[18] KLIPPEL. *NFS – Near Field Scanner manual*. Official online documentation, accessed 15 September 2026. Public double-layer separation, wave expansion and higher-frequency windowing context. No proprietary-method reconstruction or direct performance comparison is claimed.

[19] Polytec. *Laser Doppler vibrometry: technology and principles*. Official technical description, accessed 15 September 2026. Observable principle only; no instrument-specific uncertainty is assumed.

[20] Ponteggia, D. / Audiomatica. *Import CLIO 12 Binary Files with Scilab*. Official application note AN-022, revision March 2026; URL filename is Appnote_021.pdf. Time/frequency data distinction checked against the supplied historical binary audit.

[21] Li, Y., Lee, K., and Bresler, Y. "A Unified Framework for Identifiability Analysis in Bilinear Inverse Problems with Applications to Subspace and Sparsity Models." arXiv:1501.06120 (2015). Primary abstract and metadata consulted. General transformation-group perspective; acoustic counterexamples are derived in the project evidence.

[22] Luo, Z.-W., Fernandez Comesana, D., Zheng, C.-J., and Bi, C.-X. "A free field recovery technique based on the boundary element method and three-dimensional scanning measurements." *Journal of the Acoustical Society of America* 150(5), 3929 (2021). DOI: 10.1121/10.0007285. Primary abstract reviewed; flexible measurement-position formulation, not a demonstrated solution to the present acquisition.

[23] Hald, J. "Basic theory and properties of statistically optimized near-field acoustical holography." *Journal of the Acoustical Society of America* 125(4), 2105–2120 (2009). DOI: 10.1121/1.3079773. Primary abstract and metadata reviewed; finite-aperture prediction and validity-region context.